HHS Public Access

Author manuscript

Nat Immunol. Author manuscript; available in PMC 2023 May 01.

Published in final edited form as:

Nat Immunol. 2022 November ; 23(11): 1588–1599. doi:10.1038/s41590-022-01326-8.

SUSD2 suppresses CD8+ T cell antitumor immunity by targeting IL-2 receptor signaling

Bao Zhao[1,2], **Weipeng Gong**[1], **Anjun Ma**[3], **Jianwen Chen**[1], **Maria Velegraki**[2], **Hong Dong**[1], **Zihao Liu**[1], **Lingling Wang**[2,4], **Tamio Okimoto**[2,5], **Devin M. Jones**[1], **Yu L. Lei**[6], **Meixiao Long**[2,4], **Kenneth J. Oestreich**[1], **Qin Ma**[2,3], **Gang Xin**[1,2], **David P. Carbone**[2,5], **Kai He**[2,5], **Zihai Li**[2], **Haitao Wen**[1,2,*]

[1]Department of Microbial Infection and Immunity, Infectious Disease Institute, The Ohio State University, Columbus, OH, USA.

[2]Pelotonia Institute for Immuno-Oncology, The Ohio State University, Comprehensive Cancer Center, The Ohio State University, Columbus, OH, USA.

[3]Department of Biomedical Informatics, The Ohio State University, Columbus, OH, USA.

[4]Department of Internal Medicine, Division of Hematology, The Ohio State University, Columbus, OH, USA.

[5]Department of Internal Medicine, Division of Medical Oncology, The Ohio State University, Columbus, OH, USA.

[6]Department of Periodontics and Oral Medicine, University of Michigan School of Dentistry, Ann Arbor, MI, USA.

Abstract

Dysfunctional CD8$^+$ T cells, which have defective production of antitumor effectors, represent a major mediator of immunosuppression in the tumor microenvironment. Here, we showed that SUSD2 was a negative regulator of CD8$^+$ T cell antitumor function. *Susd2*$^{-/-}$ effector CD8$^+$ T cells showed enhanced production of antitumor molecules, which consequently blunted tumor growth in multiple syngeneic mouse tumor models. Through a quantitative mass spectrometry assay, we found that SUSD2 interacted with interleukin-2 receptor α (IL-2Rα) through sushi domain-dependent protein interactions and that this interaction suppressed the binding of IL-2, an essential cytokine for the effector functions of CD8$^+$ T cells, to IL-2Rα. SUSD2 was not expressed on regulatory CD4$^+$ T cells and did not affect the inhibitory function of these cells.

[*]**Correspondence:** Dr. Haitao Wen (Haitao.Wen@osumc.edu), Telephone: 614-292-6724, Fax: 614-292-9616, Address: 796 Biomedical Research Tower, 460 W 12th Ave, Columbus, OH 43210.

Author contributions

H.W. designed the experiments, supervised the study and interpreted the data. B.Z., W.G., J.C., M.V., H.D., Z.L., T.O. and D.M.J. performed experiments and provided intellectual input. A.M. and Q.M. performed key scRNA-seq analysis and provided intellectual input. L.W. and M.L. performed CAR T cell experiment and provided intellectual input. Y.L.L., K.J.O., G.X., D.P.C., K.H. and Z.L. contributed intellectual input and generated critical reagents. H.W. wrote the manuscript.

Competing interests

The authors declare no competing interests.

Reporting summary. Further information on research design is available in the Nature Research Reporting Summary linked to this article.

Adoptive transfer of *Susd2*$^{-/-}$ chimeric antigen receptor T cells induced a robust antitumor response in mice, highlighting the potential of SUSD2 as an immunotherapy target for cancer.

Despite the recent development of immune checkpoint blockade (ICB) as a revolutionizing cancer treatment, only a small fraction of patients gains sustained clinical benefit from this therapy[1]. The decline of immune function in effector CD8$^+$ T cells, a key feature of immunosuppressive tumor microenvironment (TME) in cancer patients who show resistance to ICB[2,3], is largely responsible for the failure to achieve durable clinical response. The existence of multiple immune checkpoint molecules means that individual targeting of single molecules cannot override the compensatory signals from the other inhibitory receptors[4,5] and there is an urgent need to identify new target(s) to rejuvenate CD8$^+$ T cell antitumor immunity, either alone or in combination with existing ICB treatments.

The growth factor interleukin 2 (IL-2) drives the expansion of activated human T cells[6] and regulates the effector and memory responses of mouse and human CD8$^+$ T cells[7,8]. The high-affinity IL-2 receptor (IL-2R) is a heterotrimeric complex composed of IL-2Rα, IL-2Rβ and the common γ chain[9-11]. IL-2Rα contains two sushi domains (SD), which are required for IL-2 binding with IL-2Rα[12]. IL-2Rα is required for the expansion and functions of effector and memory CD8$^+$ T cells, but not in the priming of naïve CD8$^+$ T cells[13-15]. In addition, the lack of IL-2 signaling leads to dysregulated T cell activation and autoimmunity, due to the essential role of IL-2 in the generation and maintenance of CD4$^+$ regulatory T cells (T_{reg} cells)[16]. As such, the therapeutic potential of IL-2 on CD8$^+$ T cell-mediated immunotherapy has been counteracted by the suppressive effect of T_{reg} cells on antitumor immunity[17]. Enhancement of IL-2 signaling selectively on CD8$^+$ T cells, but not T_{reg} cells, may facilitate the antitumor response of CD8$^+$ T cells.

SUSD2 is a single-pass type 1 membrane protein with a SD located on its C-terminus[18]. SDs are based on a β-sandwich structure and mediate protein-protein interaction[19]. Expression of SUSD2 has been reported in a variety of human cancers, such as breast, ovarian, non-small cell lung, gastric and colorectal cancer[20-26]. Expression of SUSD2 in cancer cells correlates either positively or negatively with tumor growth, depending on the cancer type[20-26], but the role of SUSD2 in the antitumor immunity remains unknown. Here, we found an inhibitory effect of SUSD2 on the antitumor function of CD8$^+$ T cell by modulating IL-2Rα signaling. SUSD2 was selectively expressed in effector CD8$^+$ T cells, but not in CD4$^+$ T_{reg} cells, and uniquely inhibited CD8$^+$ T cells.

Results

Antitumor immune responses are improved in *Susd2*$^{-/-}$ mice

Gene profiling assays found that high expression of SUSD2 correlated with tumor growth in an experimental colitis-associated colorectal cancer model[27]. *Susd2*$^{-/-}$ mice generated on a C57BL/6 genetic background by deleting all 15 exons of the *Susd2* gene (Extended Data Fig. 1a,b) had no apparent defects in growth and development, including fertility, breeding, body weight or behavior (data not shown). Analyses of the adaptive and innate immune system found no alteration in the number of NK1.1$^+$

NK cells, $CD3^+CD4^+$ and $CD3^+CD8^+$ T cells, $CD19^+$ B cells, $CD4^+CD25^+$ Treg cells, $CD11b^+F4/80^+$ macrophages, $CD11b^+CD11c^+$ conventional dendritic cells (DCs), $CD11b^+Ly6C^+$ monocytes or $CD11b^+Ly6G^+$ neutrophils in the spleens of naïve *Susd2*$^{-/-}$ mice (Extended Data Fig. 1c-j), suggesting no change in global immune cell populations at steady state. In multiple syngeneic mouse tumor models, including allografts of MC38 colorectal cancer (Fig. 1a), EG7 thymoma (Fig. 1b) and ovalbumin-expressing B16 (B16-OVA) melanoma (Fig. 1c) in the right flanks, tumor growth was significantly blunted in *Susd2*$^{-/-}$ mice compared to wild-type C57BL/6 mice. These observations indicated that loss of SUSD2 inhibited syngeneic tumor growth.

To examine the immune profiles in the TME, we performed single-cell RNA sequencing (scRNA-seq) in $CD45^+$ immune cells isolated from MC38 tumors in wild-type and *Susd2*$^{-/-}$ mice at day 18 post-inoculation. Unsupervised clustering identified 18 distinctive clusters that represented various immune cell populations, including macrophages, DCs, neutrophils, NK cells, T cells and B cells (Fig. 1d and Supplementary Table 1). Among the five clusters representing $CD8^+$ cells (clusters 3-7), we found opposite changes between cluster 3 and cluster 6 in *Susd2*$^{-/-}$ mice compared to wild-type mice (Fig. 1e), indicating that SUSD2 might affect the differentiation of intratumoral $CD8^+$ T cell subsets. Sub clustering of $CD8^+$ T cells indicated a substantial increase in *Ifng*$^+$ *Gzmb*$^+$ *Cx3cr1*$^+$ effector-like T cells ($CD8^+$ T_{EFF} cells, cluster 2) and a decrease in *Tcf7*$^-$ *Pdcd1*$^+$ *Havcr2*$^+$ *Lag3*$^+$ terminally exhausted T cells ($CD8^+$ T_{ExT} cells, cluster 3) in tumors from *Susd2*$^{-/-}$ mice compared to those from wild-type mice (Fig. 1f,g and Supplementary Table 2) [28-32]. We also detected decreased *Tcf7*$^+$ *Pdcd1*$^-$ *Havcr2*$^-$ naïve T cells ($CD8^+$ T_N cells, cluster 0) and slightly increased *Tcf7*$^+$ *Pdcd1*$^+$ *Havcr2*$^-$ *Lag3*$^-$ progenitor exhausted T cells ($CD8^+$ T_{ExP} cells, cluster 1) in tumors from *Susd2*$^{-/-}$ mice compared to those from wild-type mice (Fig. 1f,g). Further examination of gene signature in $CD8^+$ cells indicated increased expression of various genes encoding T cell effector molecules, such as *Gzmb* and *Ifng* in *Susd2*$^{-/-}$ $CD8^+$ cells compared to wild-type $CD8^+$ cells (Fig. 1h,i). Pathway enrichment analysis discovered higher expression of genes involved in multiple antitumor immunity-related pathways, such as cytokine-cytokine receptor interaction, in *Susd2*$^{-/-}$ $CD8^+$ cells compared to wild-type $CD8^+$ T cells (Fig. 1j). These findings suggested that SUSD2 deficiency led to an enhanced differentiation of $CD8^+$ T_{EFF} cells and reduced transition to $CD8^+$ T_{ExT} cells in the TME, which correlate with an improved control of tumor growth.

Flow cytometry analysis of MC38 tumors at day 18 post-inoculation indicated the frequencies of immune cells, including $CD11b^+F4/80^+$ macrophages, $CD11b^+CD11c^+$ DCs, $CD11b^+Ly6C^+$ monocytes, $CD11b^+Ly6G^+$ neutrophils and $NK1.1^+$ NK cells, among the $CD45^+$ tumor-infiltrating leukocytes were similar between wild-type and *Susd2*$^{-/-}$ mice (Extended Data Fig. 2a-e). In contrast, a significantly increased percentage of $CD8^+$ T cells (20% versus 14% of $CD45^+$ cells), but not $CD4^+$ T cells or $Foxp3^+$ T_{reg} cells, were detected in M38 tumors in *Susd2*$^{-/-}$ compared to wild-type C57BL/6 mice (Fig. 2a,b). The production of IFN-γ, GzmB and TNF was significantly enhanced in intratumoral $CD8^+$ T cells from *Susd2*$^{-/-}$ mice compared to wild-type mice (Fig. 2c), while intratumoral NK cells generated similar amounts of IFN-γ and $CD4^+$ T cells generated similar amounts of IFN-γ, GzmB and TNF in *Susd2*$^{-/-}$ mice and wild-type mice (Extended Data Fig. 2f,g), indicating an elevated antitumor immune response uniquely in *Susd2*$^{-/-}$ $CD8^+$ T cells. Enhanced

production of IFN-γ, GzmB and TNF in intratumoral *Susd2*$^{-/-}$ CD8^{+} T cells compared to wild-type CD8^{+} T cells was also observed in mice challenged with EG7 or B16-OVA cells (Fig. 2d,e).

Multi-dimensional flow cytometry assay with a panel of 32 lineage- and T-cell state specific markers indicated that *Susd2*$^{-/-}$ CD8^{+} T cells localized substantially more in subcluster 1 and subcluster 2, which were defined as CD8^{+} T_{EFF} cells based on the enriched expression of IFN-γ, TNF, CXCR3 and KLRG1, and less in subclusters 12, 13, 14 and 19, which were defined as CD8^{+} T_{ExT} cells, based on the high expression of Tim-3, TOX, Lag3, CD38 and CD39, compared to wild-type CD8^{+} T cells (Fig. 2f-h and Extended Data Fig. 2h,i). *Susd2*$^{-/-}$ CD8^{+} T cells were also significantly increased in subcluster 7, which was defined as TCF1^{hi}PD-1^{+}Tim-3^{-}CD8^{+} T_{EXP} cells (Fig. 2g,h). Depletion of CD8^{+} T cells completely abolished the improved control of MC38 tumor growth in *Susd2*$^{-/-}$ mice compared to wild-type mice (Fig. 2i), suggesting that enhanced CD8^{+} T_{EFF} cell function was a key contributor to the control of tumor growth in *Susd2*$^{-/-}$ mice.

Next, we asked whether *Susd2*$^{-/-}$ CD8^{+} T cells exhibited altered expression of immune checkpoint molecules[4,5]. Expression of PD-1 and LAG-3[4,28] was similar in intratumoral wild-type and *Susd2*$^{-/-}$ CD8^{+} T cells in mice challenged with MC38, EG7 or B16-OVA cells (Extended Data Fig. 2j-l). MC38 tumor growth was significantly delayed in *Susd2*$^{-/-}$ mice treated with PD-L1 Ab compared to similarly treated wild-type mice (Fig. 2j), which translated into extended survival (Fig. 2j). Despite tumor growth showing minimal response to PD-L1 Ab treatment in wild-type mice[33], tumor growth was significantly attenuated and survival was improved in PD-L1 Ab-treated *Susd2*$^{-/-}$ mice challenged with either EG7 (Fig. 2k) or B16-F10 (Fig. 2l) cells. Moreover, MC38 tumors exhibited a significantly delayed growth, alongside increased survival in *Susd2*$^{-/-}$ mice compared to wild-type mice treated with PD-1 Ab (Fig. 2m). In sum, deletion of *Susd2* synergized with PD-1 and PD-L1 blockade treatments to improve antitumor immunity.

Susd2$^{-/-}$ CD8^{+} T cells show enhanced antitumor function

Next, we examined whether SUSD2 directly modulated CD8^{+} T cell function. In various immune cell populations sorted from the spleen of naïve C57BL/6 mice, CD8^{+} T cells had the highest amount of *Susd2* transcript (Fig. 3a). Highest amounts of SUSD2 mRNA and protein were also detected in human CD8^{+} T cells isolated from peripheral blood mononuclear cells (PBMCs) (Fig. 3b,c). Stimulation with CD3-CD28 Abs induced a marked increase in the amount of *Susd2* transcript in sorted mouse CD8^{+} T cells, whereas mouse CD4^{+} T cells exhibited a moderate increase at day 3 post-stimulation (Fig. 3d,e). SUSD2 mRNA and protein were also augmented in human CD8^{+} T cells by stimulation with CD3-CD28 Abs (Fig. 3f,g). Increased *Susd2* mRNA expression was detected in CD8^{+} T cells, but not CD4^{+} T cells, infiltrating the MC38 tumors compared to splenic CD8^{+} T cells (Fig. 3h). Therefore, SUSD2 was highly expressed in mouse and human CD8^{+} T cells and its expression was further upregulated by TCR activation.

Next, we challenged total splenocytes from *Susd2*$^{-/-}$ OT-I mice with the cognate antigen peptide $OVA_{257-264}$. *Susd2*$^{-/-}$ CD8^{+} OT-I T cells generated significantly higher amounts of IFN-γ, GzmB and TNF (Fig. 3i-k and Extended Data Fig. 3a), as well as significantly

attenuated cell apoptosis, as assayed by staining with 7-AAD and annexin V, after antigen stimulation for 3 days (Fig. 3l), compared to wild-type $CD8^+$ OT-I T cells. RNA-seq in splenic $CD8^+$ T cells isolated from wild-type or *Susd2*$^{-/-}$ OT-I mice stimulated or not with $OVA_{257-264}$ for 3 days (Extended Data Fig. 3b-e and Supplementary Table 3,4) detected elevated expression of genes encoding T cell effector molecules, including *Ifng*, *Prf1*, *Tnfa*, *Gzmc*, in $OVA_{257-264}$-activated *Susd2*$^{-/-}$ compared to wild-type $CD8^+$ OT-I T cells (Extended Data Fig. 3d,e and Supplementary Table 4). *Susd2*$^{-/-}$ $CD8^+$ OT-I T cells also exhibited enhanced cytotoxicity towards OVA peptide-pulsed MC38, EG7 or B16-OVA cells compared to wild-type $CD8^+$ OT-I T cells (Fig. 3m). In antigen-presenting assay, wild-type or *Susd2*$^{-/-}$ bone marrow-derived dendritic cells (BMDCs) pulsed with $OVA_{257-264}$ were cultured with $CD8^+$ T cells isolated from wild-type or *Susd2*$^{-/-}$ OT-I mice[34]. *Susd2*$^{-/-}$ $CD8^+$ T cells generated significantly higher amounts of IFN-γ, regardless of the BMDC genotypes, compared with wild-type $CD8^+$ T cells (Extended Data Fig. 3f), suggesting the inhibitory effect of SUSD2 was intrinsic to the $CD8^+$ T cells. Production of IFN-γ, GzmB or TNF was similar in $CD4^+$ T cells isolated from wild-type or *Susd2*$^{-/-}$ OT-II mice when total splenocytes were challenged with the cognate antigen $OVA_{323-339}$ (Extended Data Fig. 4a), while *Susd2*$^{-/-}$ T_{reg} cells expressed similar amounts of Foxp3 protein (Extended Data Fig. 4b) and had a comparable capacity to block the proliferation of naïve $CD4^+$ T cells (Extended Data Fig. 4c) compared to wild-type T_{reg} cells, suggesting that loss of SUSD2 did not affect the function of $CD4^+$ T cells or T_{reg} cells.

To evaluate the antitumor function of *Susd2*$^{-/-}$ $CD8^+$ T cells *in vivo*, we primed $Thy1.2^+$ wild-type or *Susd2*$^{-/-}$ OT-I T cells with $OVA_{257-264}$ for 3 days and intravenously transferred them into $Thy1.1^+$ congenic wild-type mice challenged with EG7 tumor cells 7 days before cell transfer. While transfer of wild-type OT-I T cells resulted in reduced tumor growth compared to mice injected with PBS as control, transfer of *Susd2*$^{-/-}$ OT-I T cells led to complete eradication of EG7 tumor growth in all mice examined (Fig. 3n), suggesting a superior antitumor response by *Susd2*$^{-/-}$ compared to wild-type OT-I T cells. Transferred *Susd2*$^{-/-}$ OT-I T cells showed higher tumor infiltration and elevated production of IFN-γ, GzmB and TNF compared to wild-type OT-I T cells (Fig. 3o). Moreover, more intratumoral *Susd2*$^{-/-}$ OT-I T cells had a $TCF1^+PD\text{-}1^+T_{ExP}$ cell phenotype and a markedly decreased $TCF1^-PD\text{-}1^+Tim\text{-}3^+$ T_{ExT} cell phenotype compared to wild-type OT-I T cells (Fig. 3p,q), suggesting an attenuated transition of *Susd2*$^{-/-}$ T cells to terminal exhaustion. Collectively, these results suggested that *Susd2*$^{-/-}$ $CD8^+$ T cells provided a superior antitumor effect, presumably through enhanced production of cytotoxic factors.

SUSD2-IL-2Rα interaction requires SD

Because SUSD2 contains a short (16 amino acids) undefined cytoplasmic tail, suggesting that SUSD2 may not initiate intracellular signaling directly, we investigated whether SUSD2 modulated $CD8^+$ T cell effector function through its interaction with cell surface protein(s). To determine the interactome of SUSD2 in $CD8^+$ T cells, we retrovirally transduced *Susd2*$^{-/-}$ OT-I T cells with a V5-tagged mouse *Susd2* or empty vector as control, followed by V5 agarose immunoprecipitation and liquid chromatography coupled to tandem MS (LC-MS/MS). Susd2 was detected only in the precipitates from *Susd2*-reconstituted *Susd2*$^{-/-}$ OT-I T cells (Fig. 4a,b). IL-2Rα was highly enriched in

the precipitates from *Susd2*-reconstituted *Susd2*$^{-/-}$ OT-I cells compared to those from *Susd2*$^{-/-}$ OT-I cells reconstituted with empty vector, based on the number of peptides (indicating the identification confidence) and the number of peptide-spectrum matches (PSMs, indicating the abundance) (Fig. 4a and Supplementary Table 5). Susd2 and IL-2Rα coimmunoprecipitated from *Susd2*-reconstituted cells activated by $OVA_{257-264}$ for 3 days (Fig. 4c), while Susd2 did not pulldown IL-2Rβ, common γ chain or IL-15Rα (Fig. 4c,d), suggesting a specific interaction between Susd2 and IL-2Rα. The authenticity of the IL-2Rα band was verified by immunoblotting of 293T cells expressing Flag-tagged IL2RA (Flag-IL2RA) (Extended Data Fig. 5a) using both human IL-2Rα (sc-365511) and Flag Abs (Extended Data Fig. 5b). In 293T cells co-transfected with plasmids expressing V5-SUSD2 and Flag-IL2RA, SUSD2 co-immunoprecipitated with IL-2Rα (Fig. 4e,f) and colocalized with IL-2Rα on the cell surface (Fig. 4g). Overexpressed V5-SUSD2 also pulled down endogenous IL-2Rα in human Jurkat T cells (Fig. 4h), indicating that IL-2Rα interacted with SUSD2 in mouse and human cells.

Because both SUSD2 and IL-2Rα contain a SD (Fig. 4b), which is known to mediate protein-protein interaction[19], we next tested if the interaction between SUSD2 and IL-2Rα was mediated by the SD. In 293T cells co-expressing a SUSD2 mutant protein lacking the SD ($SUSD2^{\Delta SD}$) and IL-2Rα, we could not detect an interaction between $SUSD2^{\Delta SD}$ and IL-2Rα (Fig. 4i). Deletion of SD1 in IL-2Rα resulted in the loss of SUSD2-IL-2Rα interaction, while deletion of SD2 in IL2-Rα had no effect in 293T cells co-expressing the mutant IL-2Rα proteins and $SUSD2^{WT}$ (Fig. 4j). These observations indicated that SUSD2 interacted with IL-2Rα, and the interactions was mediated by the SD in both proteins.

SUSD2 negatively regulates IL-2R signaling

Because IL-2 signaling regulates effector function of $CD8^+$ T cells[7,8,35,36], we next investigated whether SUSD2 interfered with IL-2 signaling through the IL-2R. Stimulation of naïve $CD8^+$ T cells with the γ chain family cytokine IL-2, IL-7 or IL-15 only induced a slight increase in the expression of *Susd2*, in contrast to the strong upregulation of *Susd2* gene transcription in TCR-activated $CD8^+$ T cells (Extended Data Fig. 6a). When $OVA_{257-264}$-activated OT-I T cells were rested overnight before stimulation with either IL-2, IL-7 or IL-15[7], IL-2-treated *Susd2*$^{-/-}$ OT-I T cells showed enhanced phosphorylation of STAT5, an essential transcription factor downstream of IL-2 signaling[36], and elevated production of GzmB compared to IL-2-treated wild-type OT-I T cells (Fig. 5a,b and Extended Data Fig. 6b), while IL-7- or IL-15-treated wild-type and *Susd2*$^{-/-}$ OT-I T cells induced the same amount of p-STAT5 and GzmB (Fig. 5a,b and Extended Data Fig. 6c,d). p-STAT5 was comparable in IL-2-treated wild-type and *Susd2*$^{-/-}$ T_{reg} cells (Extended Data Fig. 6e), suggesting that SUSD2 specifically affected IL-2R signaling in $CD8^+$ T cells. Blocking Abs for IL-2 (clone JES6-1A12)[13] or IL-2Rα (clone PC61), but not blocking Abs for IL-2Rβ (clone TM-β1), abolished the elevated production of IFN-γ and GzmB in *Susd2*$^{-/-}$ OT-I T cells stimulated with a suboptimal dose (200 ng/ml) of $OVA_{257-264}$ (Fig. 5c,d). The enhanced production of IFN-γ (Extended Data Fig. 6f) and increased apoptosis (Fig. 5e) of *Susd2*$^{-/-}$ $CD8^+$ T cells cocultured with $OVA_{257-264}$-pulsed were attenuated by blocking antibodies against IL-2 or IL-2Rα, but not IL-2Rβ. Cell surface expression of IL-2Rα was similar between wild-type and *Susd2*$^{-/-}$ OT-I T cells (Fig. 5f), indicating that

enhanced IL-2 signaling in *Susd2*$^{-/-}$ OT-I T cells was not due to elevated expression of IL-2Rα.

Based on the crystal structure of IL-2 in complex with IL-2Rα, IL-2 engages IL-2Rα along the length of SD1[12]. To test the hypothesis that SUSD2 competitively blocked the SD-dependent binding of IL-2 to IL-2Rα, we performed an IL-2 binding assay using biotinylated IL-2 in 293T cells that overexpressed V5-SUSD2 and/or Flag-IL2RA. We did not detect direct binding between SUSD2 and biotinylated IL-2, but overexpression of V5-SUSD2 significantly decreased binding of biotinylated IL-2 to overexpressed Flag-IL2RA (Fig. 5g). Increased binding of biotinylated IL-2 to $OVA_{257-264}$-activated *Susd2*$^{-/-}$ OT-I T cells was observed compared to similarly-treated wild-type OT-I T cells (Fig. 5h), suggesting that SUSD2 negatively regulated IL-2R signaling by interfering with IL-2-IL-2Rα binding.

Selective targeting of IL-2/IL-2 Ab immune complexes on IL-2 receptors improves IL-2 immunotherapy against tumors[13,37,38]. To examine the impact of SUSD2 on IL-2R signaling during an antitumor response *in vivo*, we compared the efficacy of IL-2/IL-2 Ab complexes in limiting the growth of B16-F10 tumors in wild-type and *Susd2*$^{-/-}$ mice. We used an IL-2Rα-targeting complex (IL-2/Ab_{CD25}, which is mouse IL-2 complexed with IL-2 Ab, clone JES6-1A12) and a CD122-targeting complex (IL-2/Ab_{CD122}, mouse IL-2 complexed with IL-2 Ab, clone S4B6-1)[13,37]. IL-2/Ab_{CD25} had a minimal effect on tumor growth in wild-type mice compared to PBS injection, as previously reported[37] (Extended Data Fig. 6g), but significantly blunted the growth of B16-F10 tumors in *Susd2*$^{-/-}$ mice (Extended Data Fig. 6g), while IL-2/Ab_{CD122} caused a similar reduction of tumor growth in wild-type and *Susd2*$^{-/-}$ mice (Extended Data Fig. 6h). IL-2/Ab_{CD25}-treated *Susd2*$^{-/-}$ mice had significantly increased percentages of intratumoral $CD8^+$ T cells that produced IFN-γ, GzmB and TNF compared to IL-2/Ab_{CD25}-treated wild-type mice (Extended Data Fig. 6i-k). Collectively, these findings indicated an inhibitory effect of SUSD2 on IL-2R function.

SUSD2 inhibits $CD8^+$ T cell antitumor function via SD

We next inquired whether the interaction between SUSD2 and IL-2Rα was required for the inhibitory effect of SUSD2 on $CD8^+$ T cell activation. In $OVA_{257-264}$-activated *Susd2*$^{-/-}$ OT-I T cells retrovirally transduced with GFP-tagged full-length SUSD2 ($SUSD2^{FL}$-GFP), $SUSD2^{\Delta SD}$-GFP or EV-GFP with about 50% of transduction efficiency (Fig. 6a), we observed decreased production of IFN-γ and GzmB (Fig. 6b,c) and increased apoptosis (Fig. 6d) in GFP^+ OT-I T cells reconstituted with $SUSD2^{FL}$-GFP, but not with $SUSD2^{\Delta SD}$-GFP compared to cells reconstituted with EV-GFP. Moreover, transduction of *Susd2*$^{-/-}$ OT-I T cells with $SUSD2^{FL}$-GFP, but not $SUSD2^{\Delta SD}$-GFP, inhibited the binding of biotinylated IL-2 to *Susd2*$^{-/-}$ OT-I T cells (Fig. 6e) and IL-2-induced STAT5 phosphorylation (Fig. 6f). These results suggested that loss of SUSD2 interaction with IL-2Rα ablated its inhibitory effect on $CD8^+$ T cell effector function *in vitro*.

To determine whether the Susd2-IL-2Rα interaction modulated the antitumor effector function of $CD8^+$ T cells *in vivo*, we adoptively transferred $Thy1.2^+$ *Susd2*$^{-/-}$ OT-I T cells transduced with $SUSD2^{FL}$-GFP, $SUSD2^{\Delta SD}$-GFP or EV-GFP into $Thy1.1^+$ mice challenged with EG7 tumor cells 7 days before cell transfer. While $SUSD2^{FL}$-GFP *Susd2*$^{-/-}$ OT-I T

cells exhibited impaired capacity to control EG7 tumor growth, SUSD2$^{\Delta SD}$-GFP *Susd2*$^{-/-}$ OT-I T cells controlled tumor growth at levels comparable to EV-GFP *Susd2*$^{-/-}$ OT-I T cells (Fig. 6g). SUSD2^{FL}-GFP, but not SUSD2$^{\Delta SD}$-GFP *Susd2*$^{-/-}$ OT-I T cells had attenuated tumor infiltration, decreased production of IFN-γ, GzmB and TNF (Fig. 6h) and significantly decreased about 42% of CD8$^+$ T_{ExP} cell (Fig. 6i) and increased about 77% of CD8$^+$ T_{ExT} cells (Fig. 6j) compared to EV-GFP *Susd2*$^{-/-}$ OT-I T cells. This indicated that the SUSD2-IL-2Rα interaction was required for the inhibitory role of SUSD2 on the antitumor effector function of CD8$^+$ T cells (Extended Data Fig.8).

Deletion of Susd2 improves antitumor efficacy of CAR T cells

To evaluate the potential of SUSD2 as an immunotherapy target for cancer, we investigated its role in regulating the antitumor efficacy of human CD19 (hCD19)-targeting CAR T cells. The mouse EL4 thymoma cell line was engineered to express hCD19 (Extended Data Fig. 7a) and wild-type or *Susd2*$^{-/-}$ CD8$^+$ T cells were retrovirally transduced with a second-generation CAR containing a portion of hCD19 single chain variable fragment (ScFv) fused with the signaling domains from mouse CD28 and a mouse CD3ζ sequence in which the first and third ITAMs had been inactivated[39]. Sorted CAR T cells with a 98% live cell purity were transferred into *Rag2*$^{-/-}$ mice that have been inoculated with EL4-hCD19 tumor cells 7 days before CAR T cell transfer (Extended Data Fig. 7b). While wild-type CAR T cells restrained tumor growth before day 13 post tumor cell inoculation, tumor growth rebounded at day 13, leading to similar survival in *Rag2*$^{-/-}$ mice with or without wild-type CAR T cell transfer (Fig. 7a). Transfer of *Susd2*$^{-/-}$ CAR T cells significantly reduced tumor growth at day 16 post tumor cell inoculation and translated in improved survival compared to wild-type CAR T cells (Fig. 7a). We detected enhanced production of IFN-γ, GzmB and TNF as well as improved cell survival in intratumoral *Susd2*$^{-/-}$ CAR T cells compared to wild-type CAR T cells (Fig. 7b,c). Intratumoral *Susd2*$^{-/-}$ and wild-type CAR T cells had similar expression of PD-1 or LAG3 (Fig. 7d,e). As such, deletion of SUSD2 in CAR T cells lead to an improved antitumor response in an EL4-hCD19 tumor model.

Next, we depleted endogenous *Susd2* in wild-type CAR T cells using Cas9 nucleoprotein (RNP) complex electroporation[40] (Extended Data Fig. 7c). Transfer of *Susd2*-depleted CAR T cells in *Rag2*$^{-/-}$ mice resulted in improved control of EL4-hCD19 tumors and increased survival compared to transfer of wild-type CAR T cells (Fig. 7f). We observed increased production of IFN-γ, GzmB, TNF and IL-2 (Fig. 7g) and increased percentages of TCF1$^+$PD-1$^+$CD8$^+$ T_{ExP} cells and decreased percentages of TCF1$^-$PD-1$^+$Tim-3$^+$ CD8$^+$ T_{ExT} in *Susd2*-depleted CAR T cells compared to wild-type CAR T cells (Fig. 7h,i), suggesting that therapeutic deletion of SUSD2 improved effector function of CAR T cells and counteracted the differentiation of terminally exhausted CAR T cells.

Discussion

This study showed an inhibitory effect of SUSD2 on IL-2R signaling, consequently leading to an inhibition of the antitumor function of CD8$^+$ T cells. We found that SUSD2 interacted with IL-2Rα via a sushi domain-dependent manner and interfered with IL-2-mediated

effector functions of $CD8^+$ T cells. Deletion of SUSD2 in adoptively transferred T_{EFF} cells and CAR T cells led to an improved antitumor efficacy, suggesting a targetable relevance of SUSD2 in immunotherapy for cancer.

IL-2 was originally discovered as a T cell growth factor with a robust effect to promote the expansion of cytotoxic $CD8^+$ T cells[6,36]. Clinical studies revealed promising results for IL-2 therapy in cancer patients[41 42]. However, an intrinsic challenge of IL-2-based cancer immunotherapy is the activation of cytotoxic $CD8^+$ T cells in peripheral sites, which causes undesirable tissue damage. We found that, among various immune cell types, SUSD2 was highly expressed in $CD8^+$ T cells and was further upregulated when $CD8^+$ T cells migrated from the secondary lymphoid organ into the TME. Therefore, based on the inhibitory effect of SUSD2 on IL-2R signaling, blockade of SUSD2 may preferentially enhance the survival and function of antitumor $CD8^+$ T cells and avoid the activation of peripheral $CD8^+$ T cells. Meanwhile, since our current animal model employed a whole-body gene deletion strategy, we are not able to completely rule out potential function of SUSD2 in cellular compartments other than $CD8^+$ T cells. Further development of genetic model with conditional gene deletion is warranted to examine the role of SUSD2 in individual cell types.

Both experimental studies in tumor animal models and clinical cancer studies have characterized $CD8^+$ T cell exhaustion in the TME[43]. With the rapid advancement in scRNA-seq technology, compelling evidence shows the existence of distinct subtypes of exhausted $CD8^+$ T cells, namely TCF-1^+PD-1^+ Tim-3^- T_{ExP} cells and TCF-1^-PD-1^+Tim-3^+ T_{ExT} cells [30,31,44]. $CD8^+$ T_{EFF} cells with high expression of antitumor effectors, such as IFN-γ and granzymes, are critically required for the execution of the antitumor response[30-32]. Intratumoral $CD8^+$ T_{ExP} cells can either differentiate into CX_3CR1^+ $CD8^+$ T_{EFF} cells or T_{ExT} cells via distinct transcriptional, epigenetic and metabolic programs[30,31,44]. One strategy to improve $CD8^+$ T cell antitumor response might be to promote the conversion of T_{ExP} to T_{EFF} cells and minimize the differentiation of T_{ExT} cells. IL-2R signaling potently activates the effector responses of $CD8^+$ T cells[7,8] and IL-2 in combination with PD-L1 Ab therapy can rejuvenate T_{ExT} cells in a chronic virus infection model[45]. Therefore, targeting IL-2R signaling, either alone or in combination with other ICB therapies, represents a promising approach to escalate the antitumor function of $CD8^+$ T cells, while minimizing T cell exhaustion. Our scRNA-seq assay indicated an increased percentage of $CD8^+$ T_{EFF} cells and decreased percentage of T_{ExT} cells in tumor-bearing *Susd2*$^{-/-}$ mice, highlighting a promising therapeutic potential of SUSD2 to reverse T cell exhaustion.

The long-term efficacy of CAR T therapy in cancer is severely limited by the conversion of transferred T_{EFF} cells to T_{ExT} cells. An experimental approach to block the terminal exhaustion of CAR T cell would represents a promising strategy to improve the efficacy of CAR T cell therapy. We found that depletion of endogenous *Susd2* gene in wild-type CAR T cells resulted in an improved control of tumor growth, increased effector function and decreased T cell death and terminal exhaustion, providing a promising base for further investigations in human CAR T cells.

SUSD2 is also expressed in certain types of cancers[20-26]. Clinical studies have reported either positive or negative correlations between SUSD2 expression in tumor cells and

a positive prognosis in cancer patients, depending on the type of cancer[20-26]. Further investigations are required to fully characterize the role of SUSD2 in tumor cells.

In summary, our results provide a mechanistic link between the SUSD2-modulated IL-2R signaling and the antitumor effector function of $CD8^+$ T cells and expand our current understanding of molecular mechanisms driving immunosuppression in the TME. Considering the rapid advancements in the development of immunotherapy antibodies, blockade of SUSD2 by neutralizing antibody could represents a new therapeutic approach for cancer. Moreover, because SUSD2 modulates $CD8^+$ T cell effector function independently of PD-1, blockade of SUSD2 seems suitable for combinatorial therapy, especially for tumors resistant to PD-1 therapy.

Methods

Cell lines

293T (CRL-3216), MC38 (RRID: CVCL_B288), B16-F10 (CRL-6475), EL4 (TIB39), EG7 (CRL-2113), Jurkat (TIB152) and Phoenix Eco Packaging cell (CRL-3214) were purchased from ATCC, B16-OVA (SCC420) was obtained from Sigma-Aldrich and Platinum-E (Plat-E) (RV-101) was obtained from Cell Biolabs. 293T, MC38 and B16-OVA cells were cultured in DMEM medium (Gibco) supplemented with 10% fetal bovine serum (FBS; Sigma-Aldrich), 1% glutamine (Gibco), 1% sodium pyruvate, 1% non-essential amino acids (Gibco), 100 IU/ml penicillin and 100 μg/ml streptomycin (Gibco). EL4, EG7, B16-F10, and Jurkat cells were grown in RPMI-1640 (Gibco) supplemented with 10% FBS, 1% glutamine, 1% sodium pyruvate, 1% non-essential amino acids, 100 IU/mL Penicillin and 100 μg/mL Streptomycin. All cell lines were maintained at 37°C, 5% CO_2. Buffy coats from healthy donors were purchased from the Gulf Coast Regional Blood Center and PBMCs were isolated by Ficoll-Paque (17-1440-03, GE Healthcare) density centrifugation.

Mice

Susd2$^{-/-}$ mice were generated by Cyagen Biosciences using a CRISPR/Cas9-mediated genome engineering strategy (details in Extended Data Fig. 1a). C57BL/6J (000664), Thy1.1 (000406), *Rag2*$^{-/-}$ (008449) and OT-I (003831) mice were obtained from the Jackson Laboratory. OT-II mice have been previously described [46]. *Susd2*$^{-/-}$ OT-I and *Susd2*$^{-/-}$ OT-II mice were generated by crossing *Susd2*$^{-/-}$ with OT-I and OT-II mice, respectively. All mice were housed in standard rodent micro-isolator cages and acclimated to study conditions for at least 7 days before manipulation. Mice were kept in animal rooms maintained on 12 hr light/dark cycle, temperature and humidity-controlled, between68-74 °F and 30-70% respectively. All *in vivo* experiments were performed in according with the guidelines established by The Ohio State University and National Institute of Health Guide for the Care and Use of Laboratory Animals and the Institutional Animal Care and Use Committee (IACUC) (Protocol: 2018A00000022-R1).

Tumor cell inoculation

Eight to ten-week-old male and female mice were inoculated subcutaneously with 1×10^6 MC38, EG7 or B16-OVA cells in the right flank. For adoptive T cell transfer experiments, 1×10^6 EG7 cells were inoculated subcutaneously into Thy1.1 mice (day 0). On day 7 post

inoculation, mice were adoptively transferred with 4×10^6 WT or *Susd2*$^{-/-}$ OT-I T cells via tail vein. For CAR T transfer experiments, 1×10^6 EL4-hCD19 cells were inoculated subcutaneously into *Rag2*$^{-/-}$ mice (day 0). On day 7 post inoculation, mice were injected with 5×10^6 WT or *Susd2*$^{-/-}$ CAR T cells. For CD8$^+$ T cell depletion, WT or *Susd2*$^{-/-}$ mice were treated with 200 μg of control IgG (clone LTF-2, Bio X cell) or CD8 Ab (clone 2.43, Bio X cell) at day 0, 7 and 14 post tumor inoculation. For PD-L1 or PD-1 blockade, WT or *Susd2*$^{-/-}$ mice were intraperitoneally injected with 250 μg of control IgG or PD-L1 Ab (clone 10F.9G2, Bio X Cell) or PD-1 Ab (clone RMP1-14, Bio X Cell) at day 7, 10 and 13 post tumor inoculation. For IL-2/Ab complex treatment, mIL-2 (1.5 μg, Peprotech) complexed with either IL-2Ab (7.5 μg; JES6-1A12, Bio X cell) or IL-2/IL-2 Ab (7.5 μg; S4B6-1, Bio X cell) was administered intraperitoneally at day 7, 9, 11, and 13 post tumor inoculation. Tumor volume were calculated using the formula mm^3 = (Length×width×width/2).

Flow cytometry

Tumors were minced into small fragments and digested with 1 mg/mL collagenase IV and 50 U/mL DNase I for 30 min at 37°C. Samples were mechanically disaggregated and filtered with 70-μm cell strainers. Single cell suspensions were treated with purified CD16/32 Ab (clone 93; BioLegend), and then stained with fluorochrome-conjugated Abs, including CD11b, F4/80, CD11c, Ly6C, Ly6G, CD3, CD4, CD8, CD8, CD25, Thy-1.1, Thy1.2, NK1.1, CD19, PD-1 and LAG3. For intracellular staining of p-STAT5, cells were fixed with 2% paraformaldehyde for 10 min at room temperature and then incubated in pre-chilled methanol for 20 min at 4°C for permeabilization. Cells were washed 3 times with PBS containing 2% FBS and 1mM EDTA and then stained with p-STAT5 Ab. For intracellular cytokine staining of tumor-infiltrating lymphocytes, cells were stimulated *in vitro* with PMA (50 ng/ml, Sigma-Aldrich) and ionomycin (500 ng/ml, Sigma-Aldrich) in the presence of GolgiPlug and GolgiStop (BD Biosciences) for 4 h, and then surface stained as aforementioned. Cells were then fixed and permeabilized using BD Cytofix/Cytoperm (BD Biosciences) and stained with IFN-γ, GzmB, TNF and IL-2 Abs. For intranuclear Foxp3 or TCF-1 staining, single-cell suspensions were stained with Abs against cell-surface antigens as aforementioned, fixed and permeabilized using Foxp3 Fix/Perm Buffer Kit (BioLegend), followed by staining with Foxp3 Ab or TCF-1 Ab. For cell apoptosis analysis, cells were resuspended in the annexin-V Binding Buffer and then stained with annexin-V and 7-AAD viability solution (BioLegend) for 15 min at 25°C.

To characterize CD8$^+$ cells in the TME, multi-dimensional flow cytometry assay with a panel of 32 lineage- and T-cell state specific markers (CD45, CD3, CD8, CD4, CD11b, NK1.1, Foxp3, Tim-3, PD-1, CD25, CD62L, CD69, CD44, Lag3, Vista, TIGIT, CD27, CD38, CD39, KLRG1, ICOS. CD95, CD103, CXCR3, TOX, TCF-1, Ki67, EOMES, IFN-γ, TNF, GzmB) was performed, as previously described [47]. Data were acquired in a 5-Laser Cytek Aurora System. Analysis was performed using OMIQ data analysis software (www.omiq.ai) (Omiq). Uniform Manifold Approximation and Projection (UMAP) algorithm was applied for dimension reduction and visualization of the data after concatenating all samples. Cells were then clustered based on their marker expression using the FlowSOM package [48]. Heatmaps of median marker expression were generated to further

understand the features of each cluster. Differences in the abundance of the clusters between the two groups were determined with EdgeR.

Cell sorting

$CD4^+$, $CD8^+$, $CD11b^+$ and $CD19^+$ cells were sorted from mouse splenocytes. Human $CD4^+$, $CD8^+$, $CD14^+$ and $CD19^+$ cells were sorted from PBMCs. Mouse Treg cells were isolated using the Mouse $CD4^+CD25^+$ Regulatory T Cell Isolation Kit (130-091-041; Miltenyi). Human Treg cells were isolated from PBMCs by EasySep Human $CD4^+CD127^{low}CD25^+$ Regulatory T Cell Isolation Kit (18063; STEMCELL Technologies). Cells were sorted using a 100-μm chip on a MA900 Multi-Application Cell Sorter (SONY) in PBS with 2% FBS.

scRNA-seq

MC38 tumor single cell suspensions were stained with 7-AAD and CD45 Ab and sorted (BD FACSAria Fusion Cell Sorter). Live $CD45^+$ cells were processed using the inDrops V3 scRNA-seq platform, as previously described [49]. inDrops Libraries were sequenced on the NextSeq Illumina Platform, paired-end mode. The raw sequences (FASTQ format; four WT and four KO) were aligned and quantified using the CellRanger (v3.0.2) pipeline against the pre-built 10X mouse reference genome (mm10). For each dataset, a cell was considered as low quality or abnormal and removed based on (i) less than 200 expressed genes, (ii) fewer than 200 or higher than 4,000 total features, and (iii) mitochondria content higher than 90%. We then performed the integrative analysis using the Seurat (v3.0) pipeline. Data integration was performed on the top 2,000 highly variable genes in each sample via canonical correlation analysis. Cell clusters were identified using the top five principal components (PCs) with a resolution of 0.5 in Louvain clustering. All cell clusters were manually annotated according to the expression of curated marker genes. Differentially expressed genes (DEGs) were identified in each cell cluster using the Wilcoxon rank test built in Seurat, with log-fold change as 0.25 and adjusted p-value as 0.05. We further subset those cells with *Cd8a, Trbc1*, and *Trbc2* expression from the integrated data. The subset data was re-scaled and re-clustered with the top five PCs and a resolution of 0.2 in Louvain clustering, and further annotated as T_N cells, T_{EFF} cells, T_{ExP} cells, and T_{ExT} cells based on manually curated $CD8^+$ T cell markers. DEGs in the subset data were identified similarly as described above.

Bulk RNA-seq

$CD8^+$ T cells were isolated by the EasySep Mouse $CD8^+$ T Cell Isolation Kit (STEMCELL Technologies) from total splenocytes of either WT or *Susd2*$^{-/-}$ OT-I mice left untreated or stimulated with $OVA_{257\text{-}264}$ for 3 days. RNA was extracted using TRIzol Reagent (Invitrogen) and were further quantified using Qubit Fluorometer, and those with RIN values > 7 were used for RNA isolation using NEBNext Poly mRNA Magnetic Isolation Module (#E7490L, New England Biolabs, NY). Subsequently, purified mRNAs were fragmented for 10 minutes. cDNAs were synthesized and amplified for 12 PCR cycles using NEBNext® Ultra™ II Directional (stranded) RNA Library Prep Kit for Illumina (E7760L; NEB) with NEBNext Multiplex Oligos Index kit (6442L; NEB). Distributions of the template length and adapter-dimer contamination were assessed using an Agilent 2100 Bioanalyzer and High Sensitivity DNA kit (Agilent Technologies). The concentration of cDNA libraries was

determined using Invitrogen Qubit dsDNA HS reagents and read on a Qubit Fluorometer (Thermo Fisher Scientific), and cDNA libraries were paired-end 150bp format sequenced on a NovaSeq 6,000 SP system (Illumina). Bulk RNA-seq profiling was performed on eight samples (four WT and four KO). Quality control and data trimming of the raw sequences were performed via fastp (v0.23.2), and reads alignment was performed using HISAT2 (v2.1.0) to map sequence to the mouse reference (Mus_musculus. GRCm38.99). Samtools (v1.10) was used to convert and sort bam files, and subread (v2.0.1) was used to quantify reads to generate gene expression count matrix. DEG analysis was performed using DESeq2 (v1.32.0). Genes with log-fold change greater than 1.5 and p-value less than 0.05 were considered as DEGs in each comparison.

Plasmids and molecular cloning

Commercially available expression plasmids include *SUSD2* (OHu27875) from Genscript, *Susd2* (MmCD00315635) from the Dana-Farber/Harvard Cancer Center DNA Resource Core [50], *IL2RA-eGFP* (#86055) from Addgene, pCMV3-SP-N-Flag-*mIl2ra* (MG50292-NF) and pCMV3-C-Myc-MUC4 (HG16066-CM) from Sino Biological. To generate the retrovirus vector expressing *SUSD2*, *Susd2*, or *Susd2* with the deletion of sushi domain (SUSD2$^{\Delta SD}$), *SUSD2* and *Susd2* cDNA were subcloned into the pLVX-mCherry-N1 (Clontech #632562) or pMSCV-IRES-GFP II (pMIG II, Addgene #52107) with V5 and His tag. To generate Flag-*IL2RA*, *IL2RA* cDNA were subcloned into p3×Flag-CMV-7.1 vector. All primers used for cloning are listed in Table S6. To generate IL2RA$^{\Delta SD1}$ or IL2RA$^{\Delta SD2}$ mutant, Phusion Site-Directed mutagenesis Kit was used according to the manufacturer's instructions (Thermo Fisher Scientific). Primers for mutagenesis PCR are listed in Table S7. All cloned genes were checked by sequencing.

Retroviral transduction of T cells

For retrovirus generation, Plat-E cells were seeded into 10-cm dishes overnight. On the following day, plasmid encoding pMIG II EV, pMIG II-SUSD2^{FL} or pMIG II-SUSD2$^{\Delta SD}$ and packaging plasmid pCL-Eco (Addgene #12371) were mixed along with polyethylenimine (PEI) at a 3:1 = PEI:DNA ratio and added into the Plat-E cells overnight. Medium was then changed and viral supernatant was collected twice in the following 72 h. Retroviral supernatants were concentrated by PEG 8000 and immediately stored at −80°C. For retroviral transduction, OT-I T cells or Jurkat cells were plated in 6-well plates, OT-I cells stimulated with 1 μg/ml OVA$_{257-264}$ for 24 h. Viral supernatant (1:1 vol/vol ratio) and 8 μg/ml polybrene (Sigma-Aldrich) were added. Spinfection was performed at 32°C for 2 h at 800×g. Media was changed after 2 h. Transduced OT-I T cells were cultured for another 48 h with OVA$_{257-264}$ and tested in functional assays.

Antigen-presenting assay

BMDCs were loaded with 1 μg/ml OVA$_{257-254}$ at 37°C for 2 h, then washed three times with PBS to remove excessive peptide. OT-I T cells were harvested from spleens of WT or *Susd2*$^{-/-}$ mice by CD8^{+} T Cell Enrichment Kit (Miltenyi) and then co-cultured with peptide-pulsed WT or *Susd2*$^{-/-}$ BMDCs at a 5:1 ratio in 96-well plates. In some experiments, IL-2 (JES6-1A12), IL-2Rα (PC61) or IL-2Rβ (TM-β1) blocking antibody was added to the cocultures at a concentration of 10 μg/ml.

FACS-based *in vitro* killing assay

MC38, EG7 and B16-OVA cells were labeled with CFSE (C34554; Thermo Fisher Scientific), MC38 cells were pulsed with $OVA_{257-264}$ peptides at 1 μg/ml for 1 h, and used as target cells. *In vitro* activated WT or *Susd2*$^{-/-}$ OT-I cells were collected and incubated with peptide-pulsed MC38, EG7 and B16-OVA cells at different ratios for 4 h. The percentage of dead cells were measured with 7-AAD staining.

In vitro Treg cell suppression assay

A total of 1×10^5 CFSE-labeled naïve T ($CD4^+CD25^-$) cells were stimulated with 1 μg/ml anti-CD3 Ab and 1 μg/ml anti-CD28 Ab. Tregs from WT and *Susd2*$^{-/-}$ mice were isolated with the Mouse $CD4^+CD25^+$ Regulatory T Cell Isolation Kit (130-091-041, Miltenyi), and added to the culture to achieve Treg/$CD4^+$ T cell ratios of 0.0625:1 to 1:1. $CD4^+$ T cells only, without Tregs, were used as a positive control for T cell proliferation. Three days after stimulation, CFSE dilution of $CD4^+$ T cells were analyzed by FACS assay.

IL-2 binding assay

1×10^6 WT or *Susd2*$^{-/-}$ OT-I T cells were incubated with indicated concentration of biotinylated IL-2 (ACRO Biosystems) in 100 μl PBS, 0.1% BSA for 20 min at 4°C. Cells were washed 3 times with PBS and stained with streptavidin-PE (BioLegend) for 30 min at 4°C. Parallel aliquots of cells were pre-incubated with unlabeled IL-2 (500 ng/ml, Peprotech). FACS analysis was carried out on BD FACSCanto™ II Flow Cytometry (BD Biosciences).

RT-PCR

Total RNA was extracted by using Trizol reagent (Invitrogen). cDNA was synthesized with Moloney murine leukemia virus reverse transcriptase (Invitrogen) at 38°C for 60 min. RT-PCR was performed using iTaq Universal SYBR Green Supermix (Bio-Rad) in CFX Connect Real-Time PCR Detection System (Bio-Rad). The fold difference in mRNA expression between treatment groups was determined by $^{\Delta\Delta}$Ct method. The primer pair sequences of individual genes are listed in the Table S8.

Immunoprecipitation and immunoblotting

For immunoprecipitation, cells were lysed in RIPA buffer supplemented with Protease Inhibitor Cocktail. Total protein extracts were incubated with goat anti-V5 agarose (S190-119; Bethyl Laboratories) or anti-Flag M2 Affinity Gel (A2220; Sigma-Aldrich) overnight at 4°C under gentle agitation. Samples were washed 5 times with cold RIPA buffer. To elute proteins from the beads, samples were incubated with 30 μl of SDS sample buffer at 95°C for 10 min. Protein content in the supernatant was analyzed by immunoblotting. For immunoblotting, electrophoresis of proteins was performed by using the NuPAGE system (Invitrogen) according to the manufacturer's protocol. Primary Abs for immunoblotting included SUSD2 Ab (HPA004117) and FLAG M2-HRP (A8592, Sigma-Aldrich), phospho-Stat5 Ab (Tyr694) (9351, CST), Stat5 (9363, CST), IL-2Rα Ab (AF2438-SP, R&D), IL-2Rα (sc-365511), IL-2Rβ (sc-393093) and IL-15Rα (G-3) Abs

from Santa Cruz Biotechnology, V5-HRP (A00877, GenScript) and γ chain Ab (ab273023, Abcam).

Mass spectrometry assay of SUSD2 interactome

High resolution/accurate mass-based quantitative proteomics strategy was employed to identify protein-protein interactions. Briefly, immunoprecipitated (anti-V5) Susd2 complex from retrovirus-infected *Susd2*$^{-/-}$ OT-I T cells was boiled with SDS buffer followed by Suspension Trapping based on-filter digestion, as described previously [51]. The digests were desalted using C18 StageTips, dried in a SpeedVac and then resuspended in 20 μl LC buffer A (0.1% formic acid in water) for LC-MS/MS analysis. The analysis was performed using an Orbitrap Eclipse MS (Thermo Fisher Scientific) coupled with an Ultimate 3000 nanoLC system and a nanospray Flex ion source (Thermo Fisher Scientific). Peptides were first loaded onto a trap column (PepMap C18; 2 cm×100 μm I.D.) and then separated by an analytical column (PepMap C18, 3.0 μm; 20 cm×75mm I.D.) using a binary buffer system (buffer A, 0.1% formic acid in water; buffer B, 0.1% formic acid in acetonitrile) with a 165-min gradient (1% to 25% buffer B over 115 min; 25% to 80% buffer B over 10 min; back to 2% B in 5 min for equilibration after staying on 80% B for 15 min). MS data were acquired in a data-dependent top-12 method with a maximum injection time of 20 ms, a scan range of 350 to 1,800 Da, and an automatic gain control target of 1e6. MS/MS was performed via higher energy collisional dissociation fragmentation with a target value of 5e5 and maximum injection time of 100 ms. Full MS and MS/MS scans were acquired by Orbitrap at resolutions of 60,000 and 17,500, respectively. Dynamic exclusion was set to 20 s. Protein identification and quantitation were performed using the MaxQuant-Andromeda software suite (version 1.6.3.4) with most of the default parameters [52]. An UniProt mouse database (17,089 sequences) was used for the protein identification. Other parameters include: trypsin as an enzyme with maximally two missed cleavage sites; protein N-terminal acetylation and methionine oxidation as variable modifications; cysteine carbamidomethylation as a fixed modification; peptide length must be at least 7 amino acids. False discovery rate was set at 1% for both proteins and peptides.

CAR T cell transfer

The EL4-hCD19 cell line was constructed by transfecting the EL4 cells with a MMLV retrovector carrying hCD19 with the deletion of its intracellular domain. The plasmid was packaged in the Phoenix Eco cell line and viral supernatant was harvested 48 h after transfection. After viral transduction, EL4-hCD19 were sorted to achieve the positive clone >95%. To generate hCD19-targeting CAR T cells, the CAR construct was pieced together using portions of hCD19 ScFv, and portions of the murine CD28 and CD3ζ sequences (with first and third ITAMs of the CD3-ζ molecule inactivated), and cloned into a MSGV retrovector, as previously described [53]. The retroviral vector was transfected to the Phoenix Eco cell line. The harvest, stimulation and transfection of T cells were conducted. In brief, T cells were isolated from spleens of WT or *Susd2*$^{-/-}$ mice using the EasySep Mouse T Cell Isolation Kit (STEMCELL Technologies), and then stimulated by Concanavalin A in IMDM (Gibco) with 50 μM 2-mercaptoethanol, 50 U/ml IL-2, 10 ng/ml IL-7 and 10 ng/ml IL-15 at 37°C for 24 h. On the following day, viral supernatant was spun at 2000×g, 32°C, for 2

h on RetroNectin (Takara Bio)-coated plate. Activated T cells were loaded to the plate and expanded for 2-3 days.

Deletion of endogenous *Susd2* gene in WT CAR T cells was achieved by Cas9 nucleoprotein (RNP) complex electroporation using the Neon Transfection System (MPK5000; Thermo Fisher Scientific), as previously described [40]. Before electroporation, *Susd2* crRNA (AGTGCCGTAGTATTGCCAAT) or negative control crRNA (#1072544; IDT) was mixes with Alt-R tracrRNA (#1075927; IDT) at 1:1 ratio (final concentration was 44 μM), heat at 95°C for 5 min, cooled to 78°C with −2°C/second ramp rate, 78°C for 10 min, cooled down to 25°C with −0.1°C/second ramp rate, 25°C for 5 min. Cas9 protein (3 μg, A36498; Thermo Fisher Scientific) was mixed with 1.3 μL annealed crRNA:tracrRNA duplex and incubated at room temperature for 20 min. 5×10^5 of expanded CAR T cells were resuspended in 9 μL Buffer R per electroporation, and then mixed with RNP complex and 2 μL Alt-R Cas9 Electroporation Enhancer (#2075915; IDT). 10 μL of cell:RNP mixture was loaded into the Neon pipette without any bubbles. The tip of the loaded Neon pipette was inserted into the pipette station. The setup of the electroporation parameter was 1400 V, 50 ms for 1 plus. After electroporation, cells were transferred to a 24-well plate with prewarmed media and cultured overnight. 24 h after electroporation, *Susd2*$^{-/-}$ CAR T cells were sorted by using a 100-μm chip on a MA900 Multi-Application Cell Sorter (SONY).

Statistics analysis

Data were analyzed on GraphPad Prism 8 (GraphPad Software) and R software v4.1.2. The statistical tests, n values, replicate experiments and *P* values are all indicated in the figures and/or legends. P values were calculated using two-tailed student's *t* test, one-way ANOVA or two-way ANOVA with Tukey's multiple comparisons test, log-rank (Mantel-Cox) test for Kaplan-Meier survival analysis, two-way ANOVA with Sidak's multiple comparisons test or Tukey's multiple comparisons test, Hypergeometric test and adjusted with Benjamini-Hochberg method correction and two-sided Wilcoxon's rank-sum test and adjusted with Bonferroni's correction. Differences between groups are shown as the mean ± SD.

Data distribution was assumed to be normal but this was not formally tested.

Extended Data

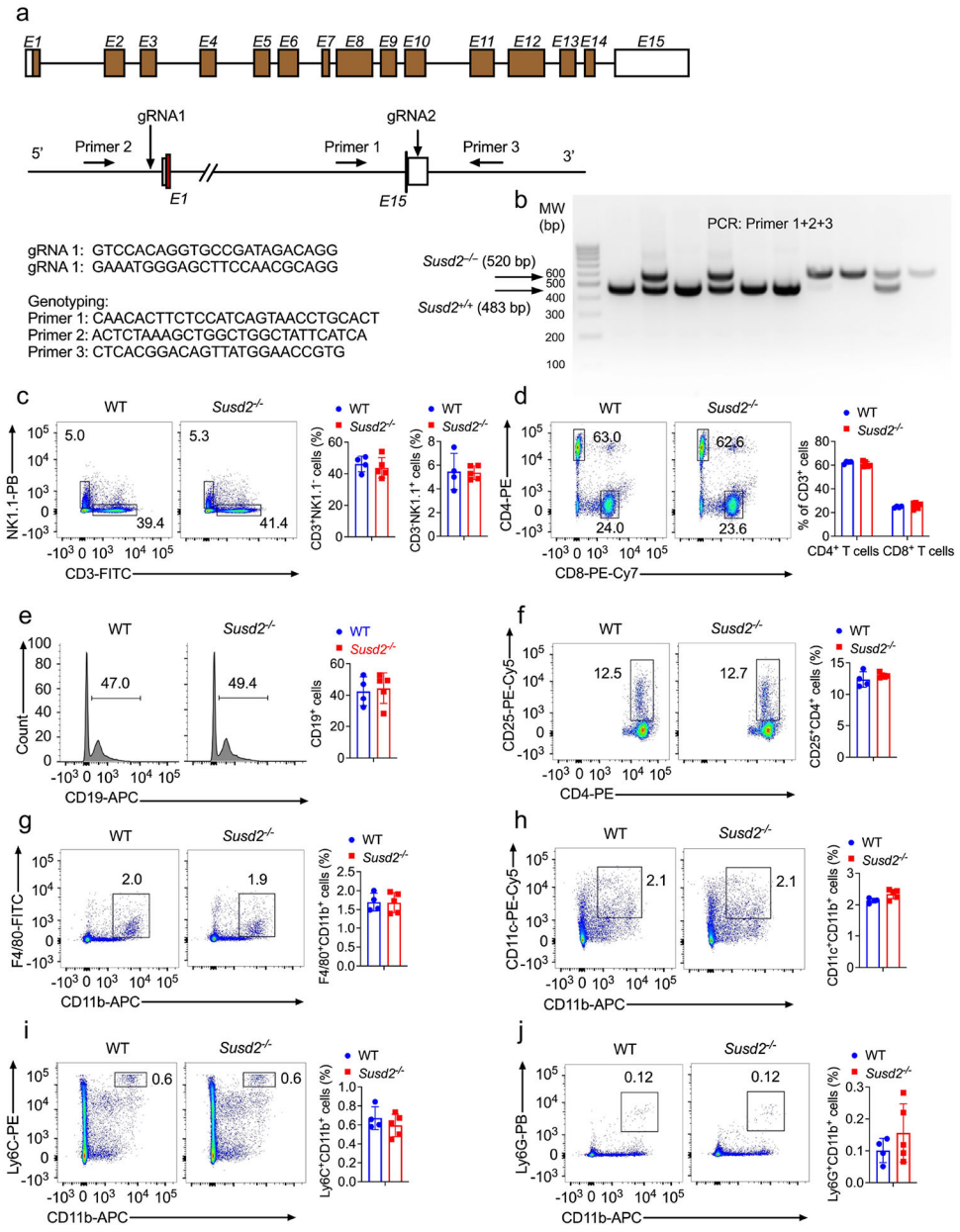

Extended Data Fig. 1. *Susd2*$^{-/-}$ mice show no change in global immune cell populations at steady state.

a, Cartoon of the strategy to generate *Susd2*$^{-/-}$ mice with a CRISPR/Cas9-mediated genome engineering strategy. The sequences of two guide RNA and the primers used for genotyping were shown. **b,** Genotyping results for WT or *Susd2*$^{-/-}$ alleles. **c-j,** Flow cytometry analysis of T cells (CD3$^+$) and natural killer cells (NK1.1$^+$) **(c),** CD4$^+$ and CD8$^+$ T cells **(d),** regulatory T cells in naïve status (CD4$^+$CD25$^+$) **(f),** macrophage (CD11b$^+$F4/80$^+$) **(g),** conventional dendritic cells (CD11b$^+$CD11c$^+$) **(h),** monocytes (CD11b$^+$Ly6C$^+$) **(i),** neutrophils (CD11b$^+$Ly6G$^+$) **(j),** and histogram of B cells (CD19$^+$) **(e)** in spleen from wild type and *Susd2*$^{-/-}$ mice were. **c-j,** WT, $n = 4$ mice, *Susd2*$^{-/-}$, $n = 5$ mice. **b-j,** data are

representative of three independent experiments. Statistical significance was determined by two-tailed, unpaired Student's *t*-test, there is no significant difference between WT and *Susd2*$^{-/-}$ in **c-j** ($P > 0.05$). All data are mean ± SD.

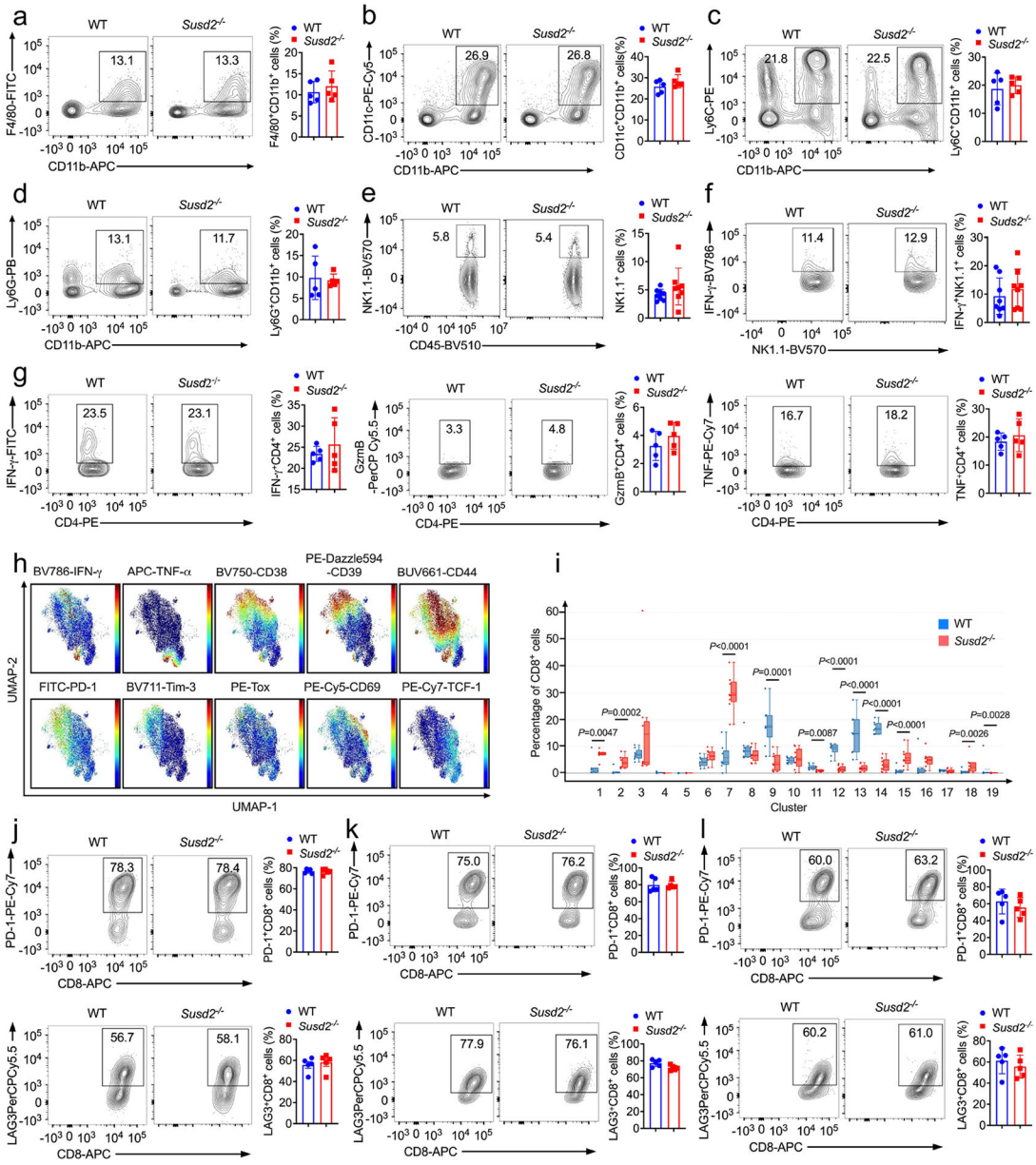

Extended Data Fig. 2. *Susd2* deficiency does not affect intratumoral myeloid cells, NK cells and CD4$^+$ T cells.

a-g, Flow cytometry analysis of CD11b$^+$F4/80$^+$ macrophages **(a),** CD11b$^+$CD11c$^+$ dendritic cells **(b),** CD11b$^+$Ly6C$^+$ monocytes **(c),** CD11b$^+$Ly6G$^+$ neutrophils **(d),** NK1.1$^+$ NK cells **(e),** IFN-γ$^+$NK1.1$^+$ NK cells **(f),** IFN-γ$^+$CD4$^+$, GzmB$^+$CD4$^+$ and TNF$^+$CD4$^+$ T cells **(g)** in MC38 tumor isolated from WT or *Susd2*$^{-/-}$ mice at Day 18. **h,i,** Spectral flow cytometry analysis of intratumor CD8$^+$ T cells from WT and *Susd2*$^{-/-}$ mice at day18 post MC38 tumor inoculation. UMAP of individual marker expression patterns **(h)** and frequencies of

individual clusters of WT and *Susd2*$^{-/-}$ samples **(i),** Boxes represent median and 25th to 75th percentiles, whiskers are minimum to maximum values excluding outliers (two-sided Wilcoxon's rank-sum *P* value). **j-l,** Flow cytometry analysis of PD-1^{+}CD8^{+} T cells and LAG-3^{+}CD8^{+} T cells in MC38 **(j),** EG7 **(k)** or B16-OVA **(l)** tumors isolated from WT or *Susd2*$^{-/-}$ mice at day 18 post tumor inoculation. **a-d,g,j-l,** $n = 5$, **e,f,i,** $n = 8$. *n*, number of mice per group. **a-d,g,j,k,l,** data are representative of three independent experiments. **e,f,i,** data are representative of two independent experiments. **a-g, j-l,** statistical significance was determined by two-tailed, unpaired Student's *t*-test, there is no significant difference between WT and *Susd2*$^{-/-}$ group (P>0.05). All data are mean ± SD.

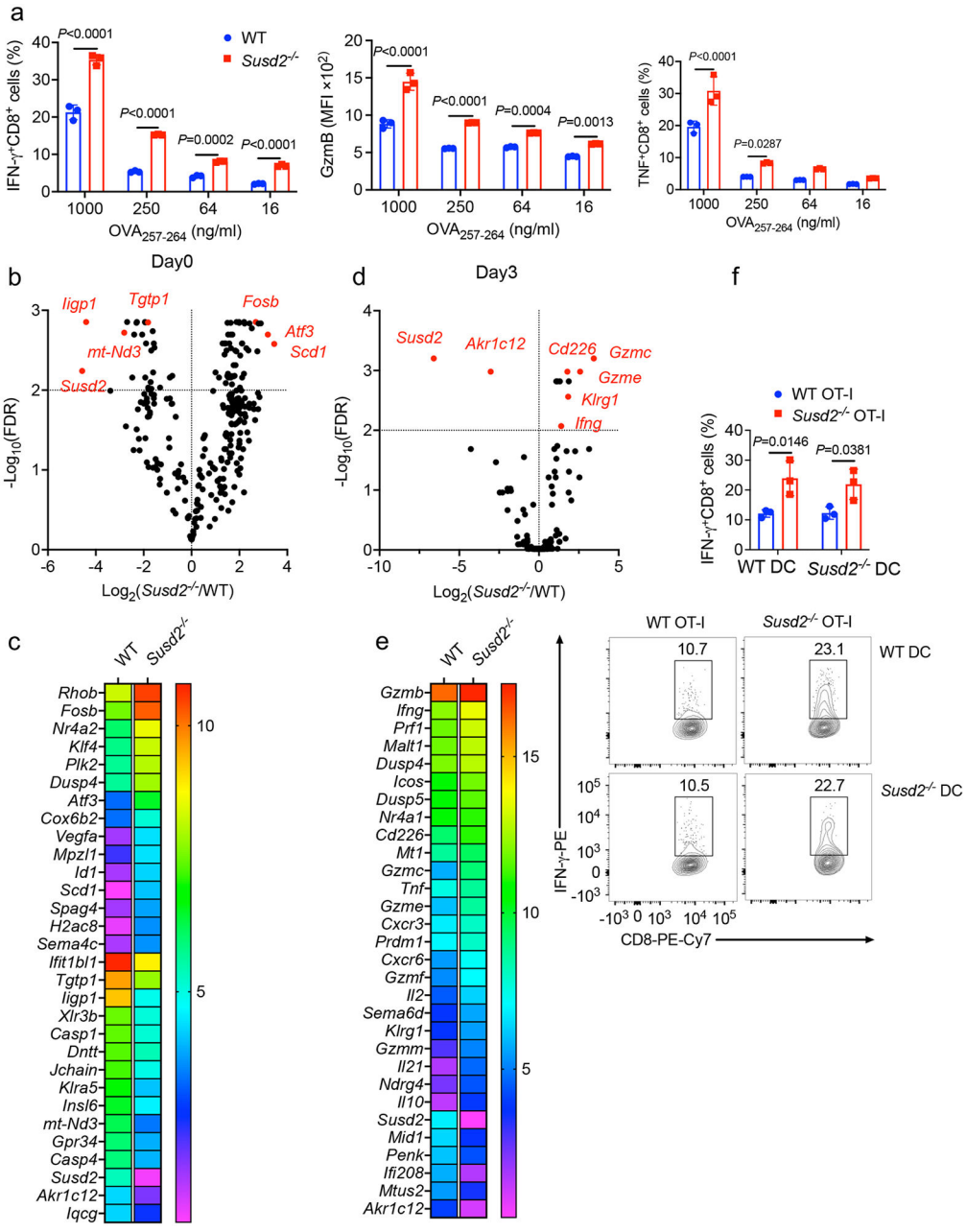

Extended Data Fig. 3. *Susd2*$^{-/-}$ CD8^{+} cells exhibit increased antitumor effector function.

a, Flow cytometry analysis of IFN-γ^{+}CD8^{+} T cells, GzmB^{+}CD8^{+} T cells and TNF^{+}CD8^{+} T cells in different $OVA_{257-264}$ dosage stimulated splenocytes isolated from WT or *Susd2*$^{-/-}$ OT-I mice. **b-e,** CD8^{+} T cells were isolated from total splenocytes of either WT or *Susd2*$^{-/-}$ OT-I mice left untreated or stimulated with $OVA_{257-264}$ for 3 days and were subjected to RNA-seq assay. The volcano plot of RNA-seq data demonstrates differential gene expression between WT and *Susd2*$^{-/-}$ CD8^{+} T cells at Day 0 **(b)** and Day 3 **(d).** A heatmap of the top thirty genes representing genes differentially expressed between WT and *Susd2*$^{-/-}$ CD8^{+} T cells at Day 0 **(c)** and Day 3 **(e). f,** Intracellular accumulation of IFN-γ in CD8^{+} T cells isolated from WT or *Susd2*$^{-/-}$ OT-I mice that were cocultured with either WT or *Susd2*$^{-/-}$ bone marrow-derived dendritic cells (BMDCs) that have been pulsed with $OVA_{257-264}$. **a,f,** $n = 3$. **b-e,** $n = 4$. n, number of mice per group. **a,f,** data are representative of four independent experiments. **b-e,** data are representative of two independent experiments. **b,d** statistical significance was calculated using two-sided Wilcoxon's rank-sum test and adjusted with Bonferroni's correction. Statistical significance was determined by two-way ANOVA followed by Sidak's multiple comparisons test**(a,f)** with P values noted in the figure. All data are mean ± SD.

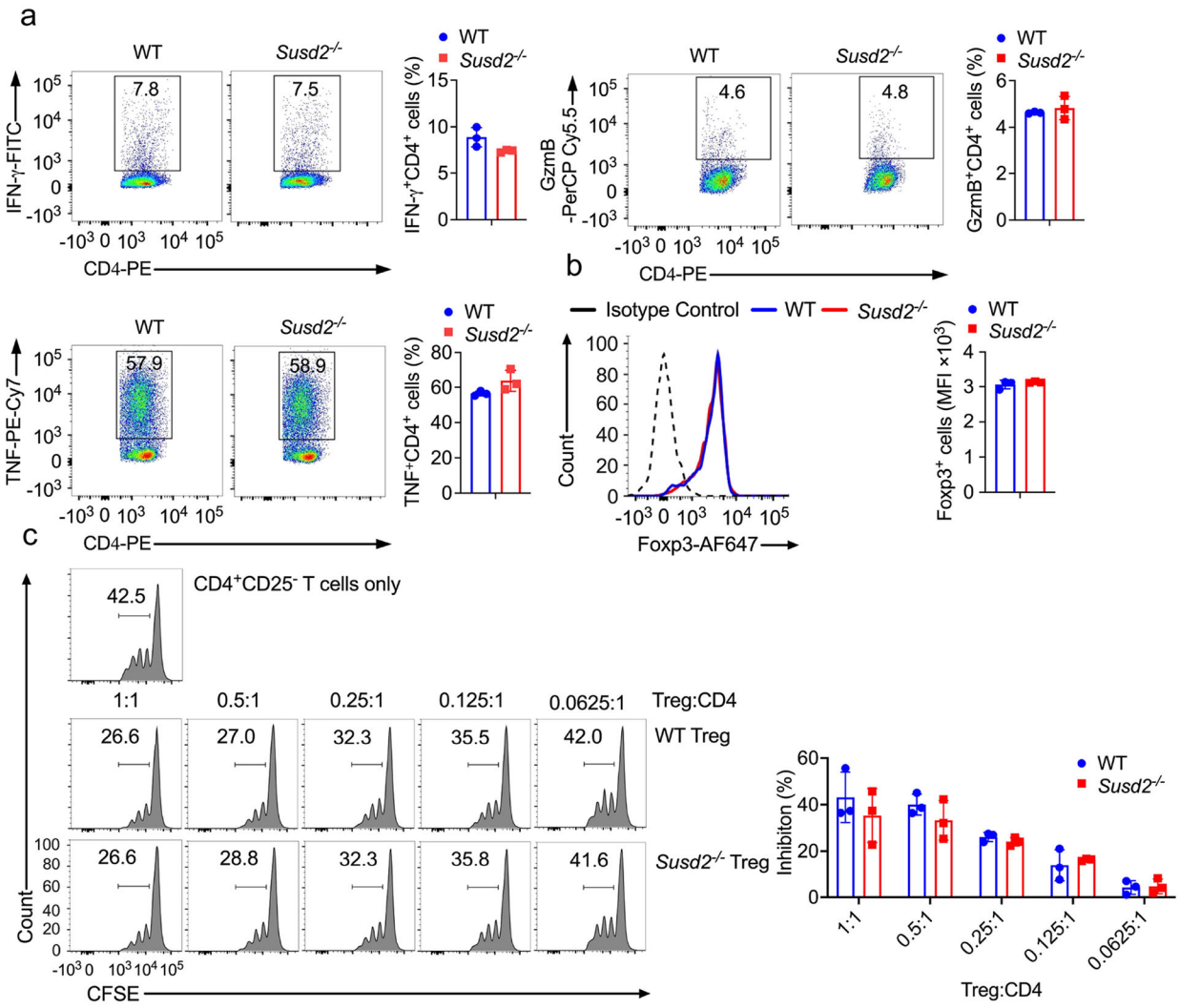

Extended Data Fig. 4. *Susd2* deficiency does not affect effector function of CD4$^+$ T cells or inhibitory function of Treg cells.

a, Flow cytometry analysis of IFN-γ$^+$CD4$^+$ T cells, GzmB$^+$CD4$^+$ T cells and TNF$^+$CD4$^+$ T cells in $OVA_{323-339}$ stimulated splenocytes isolated from WT or *Susd2*$^{-/-}$ OT-II mice. **b,** Flow cytometry analysis of intranuclear level of Foxp3 in spleen CD4$^+$ T cells from WT or *Susd2*$^{-/-}$ mice. **c,** Cell proliferation of naïve CD4$^+$ T cells upon stimulation with CD3-CD28 antibody in the absence or presence of WT or *Susd2*$^{-/-}$ Treg cells at the indicated cell: cell ratio was measured by the staining of carboxyfluorescein diacetate succinimidyl ester (CFSE), followed by FACS analysis. **a-c,** $n = 3$. n, number of mice per group. Data are representative of four independent experiments. Statistical significance was determined by two-tailed, unpaired Student's t-test, there is no significant difference between WT and *Susd2*$^{-/-}$ group in **a-c** (P>0.05). All data are mean ± SD.

a

Human *IL2RA* sequencing:

CAATGGGAGCAATAGCAGAGCTCGTTTAGTGACCGTCAGAATTAACCATG**GACTACAAAGACCATGA**
CGGTGATTATAAAGATCATGACATCGATTACAAGGATGACGATGACAAGCTTGCGGCCGCGAATTCA
ATGGATTCATACCTGCTGATGTGGGGACTGCTCACGTTCATCATGGTGCCTGGCTGCCAGGCAGAGCT
CTGTGACGATGACCCGCCAGAGATCCCACACGCCACATTCAAAGCCATGGCCTACAAGGAAGGAACC
ATGTTGAACTGTGAATGCAAGAGAGGTTTCCGCAGAATAAAAAGCGGGTCACTCTATATGCTCTGTACA
GGAAACTCTAGCCACTCGTCCTGGGACAACCAATGTCAATGCACAAGCTCTGCCACTCGGAACACAAC
GAAACAAGTGACACCTCAACCTGAAGAACAGAAAGAAAGGAAAACCACAGAAATGCAAAGTCCAATGC
AGCCAGTGGACCAAGCGAGCCTTCCAGGTCACTGCAGGGAACCTCCACCATGGGAAAATGAAGCCAC
AGAGAGAATTTATCATTTCGTGGTGGGGCAGATGGTTTATTATCAGTGCGTCCAGGGATACAGGGCTC
TACACAGAGGTCCTGCTGAGAGCGTCTGCAAAATGACCCACGGGAAGACAAGGTGGACCCAGCCCCA
GCTCATATGCACAGGTGAAATGGAGACCAGTCAGTTTCCAGGTGAAGAGAAGCCTCAGGCAAGCCCC
GAAGGCCGTCCTGAGAGTGAGACTTCCTGCCTCGTCACAACAACAGATTTTCAAATACAGACAGAAAT
GGCTGCAACCATGGAGACGTCCATATTTACAACAGAGTACCAGGTAGCAGTGGCCGGCTGTGTTTTCC
TGCTGATCAGCGTCCTCCTCCTGAGTGGGCTCACCTGGCAGCGGAGACAGAGGAAGAGTAGAAGAAC
AATCTAGTCTAGAGGATCCCGGGTGGCATCCCTGTGACCCCTCCCCAGTGCCTCTCCTGGCCCTGGA
AGTTGCCACTCCAGTGCCCACCAGCCTTGTCCTAATAAAATTAAGTTGCATCATTTTGTCTGACTAGGT
GTCCTTCTATATATTATGGGGTGGAGGGGGGKGKGGWWWKGRRSCAAGGGGCAAGTTGGGAAGAMA
CCTGTAGGGCCTGCGGGTYTATTGGGAACCAAGCTGGAGTGCAGKGCACATCTGGCTCMCTGCATCT
CCGCCTCCTGGGTCAGCGATCTCCTGCCTCAGCCTCCCGAGTTGTGGGATTCAGGCATGCATGACAG
GCTCAGCTATTTTTGTTTTTTGTARRACGGTTTCACCATATTGGCAGCTGGTCTCCACTCCTATYYCAG
GKGATCTACCCACCTTGGCCTCCAAA

Underline: 3×Flag tag; ATG and TAG represent the start and stop codon, respectively.

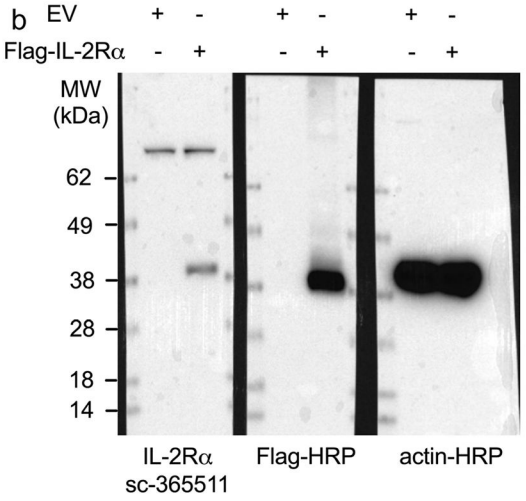

Extended Data Fig. 5. The authenticity of the IL-2Rα molecular weight.

a, Sanger sequencing result of pCMV3×Flag-IL2RA vector. **b,** Immunoblotting of Flag-IL2Rα in 293T cells transfected with pCMV3×Flag-*IL2RA* vector. Data are representative of three independent experiments.

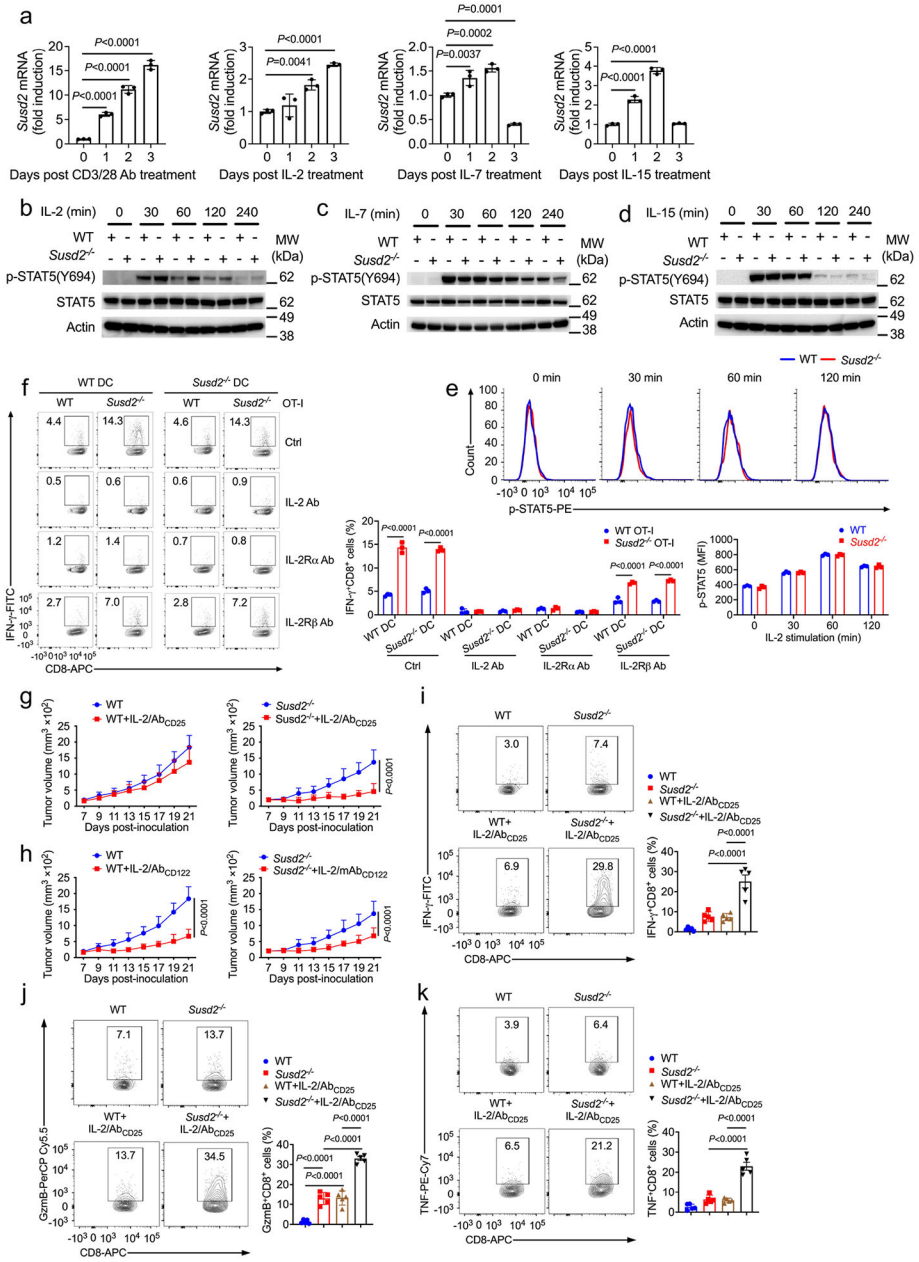

Extended Data Fig. 6. Efficient control of tumor growth by IL-2/mAb$_{CD25}$ complex in *Susd2*$^{-/-}$ mice

a, Transcript of *Susd2* in mouse CD8$^+$ T cells stimulated with CD3-CD28 Ab, IL-2, IL-7 or IL-15 for 0, 1, 2 and 3 days. **b-d,** Immunoblotting of STAT5 in OVA$_{257-264}$-primed WT or *Susd2*$^{-/-}$ OT-I T cells which were rested overnight, and then stimulated with IL-2 (100 U/ml), IL-7 (5 ng/ml) or IL-15 (10 ng/ml) for 0, 30, 60, 120 and 240 minutes. **e,** Flow cytometry analysis of p-STAT5 in WT or *Susd2*$^{-/-}$ Treg cells stimulated with IL-2 (100 U/ml) for 0, 30, 60 and 120 minutes. **f,** CD8$^+$ T cells isolated from WT or *Susd2*$^{-/-}$ OT-I mice were cocultured with WT or *Susd2*$^{-/-}$ bone marrow-derived dendritic cells (BMDCs) that have been pulsed with OVA$_{257-264}$. Intracellular accumulation of IFN-γ in WT or *Susd2*$^{-/-}$ CD8$^+$ T cells in the absence or presence of blocking antibodies against IL-2,

IL-2Rα, or IL-2Rβ were measured by FACS analysis. **g,h,** Tumor growth in WT and *Susd2*$^{-/-}$ mice bearing B16-F10 tumor cells which were injected with IL-2/Ab$_{CD25}$ complex **(g)** or IL-2/Ab$_{CD122}$ complex**(h). i-k,** Flow cytometry analysis of intracellular accumulation of IFN-γ, GzmB and TNF-expressing intratumoral CD8$^+$ T cells. **a,e,f,** $n = 3$; **g-k,** $n = 5$. *n*, number of mice per group. **a-h,** data are representative of three independent experiments; **i-k,** data are representative of two independent experiments. Statistical significance was determined by two-way ANOVA followed by Sidak's multiple comparisons test **(e-g)** or one-way ANOVA followed by Tukey's test **(a,i-k)** with *P* values noted in the figure. All data are mean ± SD.

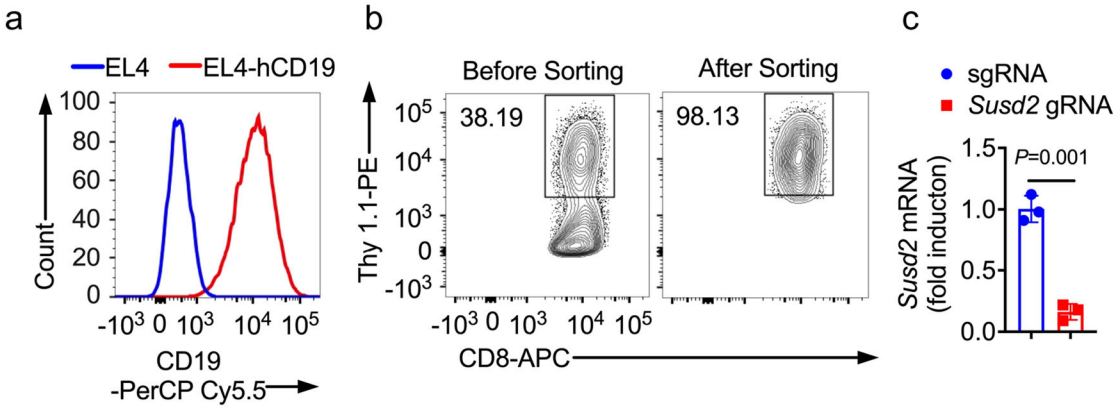

Extended Data Fig. 7. Identification of EL4-hCD19 cells and CAR T cells.

a, Validation of EL4 thymoma cell line expressing human CD19 (EL4-hCD19) with the deletion of its intracellular domain. **b,** Percentages of CD8$^+$ T cells retrovirally transduced with a chimeric antigen receptor (CAR) containing a portion of hCD19 single chain variable fragment (ScFv) fused with signaling domains of mouse CD28 and mouse CD3ζ sequence (with first and third ITAMs of the CD3ζ molecule inactivated) before and after cell sorting were assessed by the staining with anti-Thy1.1 antibody. **c,** Transcript of *Susd2* in CAR T cells that have been electroporated with scrambled gRNA(sgRNA) or Susd2 gRNA-Cas9 nucleoprotein (RNP) complex, sgRNA versus *Susd2* gRNA (P=0.0010). **c,** $n = 3$. **a-c,** data are representative of two independent experiments. Statistical significance was determined by two-tailed, unpaired Student's *t*-test **(c)** with *P* values noted in the figure. The data represent mean ± SD.

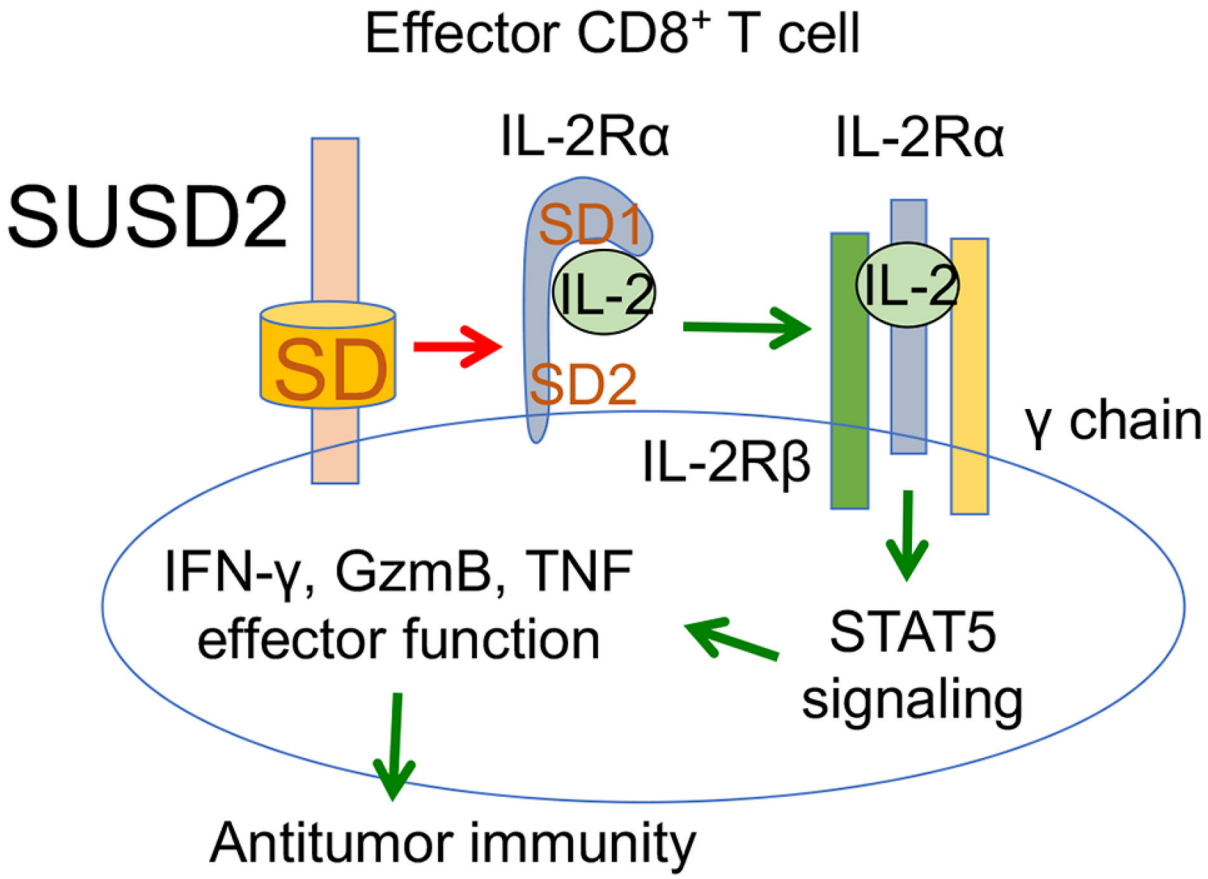

Extended Data Fig. 8. A model for an inhibitory role of SUSD2 in effector CD8$^+$ T cell antitumor immunity by modulating IL-2R signaling.

The present study has identified SUSD2 as a negative regulator of IL-2-mediated effector CD8$^+$ T cell functions and antitumor immunity. Both SUSD2 and IL-2Rα chain (IL-2Rα) contain the sushi domain (SD). Genetic ablation of SUSD2 (*Susd2*$^{-/-}$) leads to elevated IFN-γ, GzmB and TNF production in effector CD8$^+$ T cells and improved tumor growth control in multiple syngeneic tumor models. Mechanistically, SD-dependent interaction between SUSD2 and IL-2Rα competitively inhibits IL-2-IL-2Rα binding, leading to an attenuated IL-2R signaling. Therefore, SUSD2 represents a promising therapeutic target of tumor immunotherapy. Green and red arrows indicate promoting and inhibiting effect, respectively.

Supplementary Material

Refer to Web version on PubMed Central for supplementary material.

Acknowledgments

We thank members of the Wen lab for discussion; Y. Wan for critical feedback; M. Croft for the OT-II mice; Y. Fu for the MC38 cell line; Y. Yu from the University of Delaware Mass Spectrometry Core Facility for the assistance of mass spectrometry assay; P. Yan and X. Chen from the Genomics Shared Resource at the Ohio State University for the assistance of bulk RNA-seq and scRNA-seq assay. This work was supported by National Institutes of Health (NIH) grants R01GM135234 and R01AI162779 (H.W.), R01AI077283 and R01CA262089 (Z.L.), R01GM131399

(Q.M.), R01DE026728 (Y.L.), R01AI134972 (K.J.O.) and The Ohio State University Comprehensive Cancer Center Intramural Research Program (A.M., D.M.J., K.H. and H.W.).

Data availability

ScRNA-seq and bulk RNA-seq data reported in this paper are accessible at the Gene Expression Omnibus under accessions GSE210704 and GSE212179, respectively. MS data have been deposited in an international public repository (MassIVE proteomics repository at https://massive.ucsd.edu/) under data set accession number MSV000087205. There are no restrictions for data availability. Source data are provided with this paper.

References

1. Schoenfeld AJ & Hellmann MD Acquired Resistance to Immune Checkpoint Inhibitors. Cancer Cell 37, 443–455 (2020). [PubMed: 32289269]
2. Altorki NK, et al. The lung microenvironment: an important regulator of tumour growth and metastasis. Nature reviews 19, 9–31 (2019).
3. Binnewies M, et al. Understanding the tumor immune microenvironment (TIME) for effective therapy. Nat Med 24, 541–550 (2018). [PubMed: 29686425]
4. Andrews LP, Yano H & Vignali DAA Inhibitory receptors and ligands beyond PD-1, PD-L1 and CTLA-4: breakthroughs or backups. Nat Immunol 20, 1425–1434 (2019). [PubMed: 31611702]
5. Kalbasi A & Ribas A Tumour-intrinsic resistance to immune checkpoint blockade. Nat Rev Immunol 20, 25–39 (2020). [PubMed: 31570880]
6. Morgan DA, Ruscetti FW & Gallo R Selective in vitro growth of T lymphocytes from normal human bone marrows. Science 193, 1007–1008 (1976). [PubMed: 181845]
7. Pipkin ME, et al. Interleukin-2 and inflammation induce distinct transcriptional programs that promote the differentiation of effector cytolytic T cells. Immunity 32, 79–90 (2010). [PubMed: 20096607]
8. Kalia V, et al. Prolonged interleukin-2Ralpha expression on virus-specific CD8+ T cells favors terminal-effector differentiation in vivo. Immunity 32, 91–103 (2010). [PubMed: 20096608]
9. Boyman O & Sprent J The role of interleukin-2 during homeostasis and activation of the immune system. Nat Rev Immunol 12, 180–190 (2012). [PubMed: 22343569]
10. Leonard WJ, Lin JX & O'Shea JJ The gammac Family of Cytokines: Basic Biology to Therapeutic Ramifications. Immunity 50, 832–850 (2019). [PubMed: 30995502]
11. Wang X, Rickert M & Garcia KC Structure of the quaternary complex of interleukin-2 with its alpha, beta, and gammac receptors. Science 310, 1159–1163 (2005). [PubMed: 16293754]
12. Rickert M, Wang X, Boulanger MJ, Goriatcheva N & Garcia KC The structure of interleukin-2 complexed with its alpha receptor. Science 308, 1477–1480 (2005). [PubMed: 15933202]
13. Boyman O, Kovar M, Rubinstein MP, Surh CD & Sprent J Selective stimulation of T cell subsets with antibody-cytokine immune complexes. Science 311, 1924–1927 (2006). [PubMed: 16484453]
14. Williams MA, Tyznik AJ & Bevan MJ Interleukin-2 signals during priming are required for secondary expansion of CD8+ memory T cells. Nature 441, 890–893 (2006). [PubMed: 16778891]
15. Bachmann MF, Wolint P, Walton S, Schwarz K & Oxenius A Differential role of IL-2R signaling for CD8+ T cell responses in acute and chronic viral infections. Eur J Immunol 37, 1502–1512 (2007). [PubMed: 17492805]
16. Malek TR The biology of interleukin-2. Annu Rev Immunol 26, 453–479 (2008). [PubMed: 18062768]
17. Scott EN, Gocher AM, Workman CJ & Vignali DAA Regulatory T Cells: Barriers of Immune Infiltration Into the Tumor Microenvironment. Front Immunol 12, 702726 (2021). [PubMed: 34177968]
18. Sugahara T, et al. Isolation of a novel mouse gene, mSVS-1/SUSD2, reversing tumorigenic phenotypes of cancer cells in vitro. Cancer Sci 98, 900–908 (2007). [PubMed: 17428258]

19. Souri M, Kaetsu H & Ichinose A Sushi domains in the B subunit of factor XIII responsible for oligomer assembly. Biochemistry 47, 8656–8664 (2008). [PubMed: 18652485]
20. Watson AP, Evans RL & Egland KA Multiple functions of sushi domain containing 2 (SUSD2) in breast tumorigenesis. Mol Cancer Res 11, 74–85 (2013). [PubMed: 23131994]
21. Pan W, et al. CSBF/C10orf99, a novel potential cytokine, inhibits colon cancer cell growth through inducing G1 arrest. Sci Rep 4, 6812 (2014). [PubMed: 25351403]
22. Cai C, et al. Reduced expression of sushi domain containing 2 is associated with progression of non-small cell lung cancer. Oncol Lett 10, 3619–3624 (2015). [PubMed: 26788179]
23. Sheets JN, et al. SUSD2 expression in high-grade serous ovarian cancer correlates with increased patient survival and defective mesothelial clearance. Oncogenesis 5, e264 (2016). [PubMed: 27775699]
24. Hultgren EM, Patrick ME, Evans RL, Stoos CT & Egland KA SUSD2 promotes tumor-associated macrophage recruitment by increasing levels of MCP-1 in breast cancer. PLoS One 12, e0177089 (2017). [PubMed: 28475599]
25. Zhang S, et al. Downregulation of endometrial mesenchymal marker SUSD2 causes cell senescence and cell death in endometrial carcinoma cells. PLoS One 12, e0183681 (2017). [PubMed: 28841682]
26. Umeda S, et al. Expression of sushi domain containing two reflects the malignant potential of gastric cancer. Cancer Med 7, 5194–5204 (2018). [PubMed: 30259711]
27. Li X, et al. Myeloid-derived cullin 3 promotes STAT3 phosphorylation by inhibiting OGT expression and protects against intestinal inflammation. J Exp Med 214, 1093–1109 (2017). [PubMed: 28280036]
28. McLane LM, Abdel-Hakeem MS & Wherry EJ CD8 T Cell Exhaustion During Chronic Viral Infection and Cancer. Annu Rev Immunol 37, 457–495 (2019). [PubMed: 30676822]
29. Miller BC, et al. Subsets of exhausted CD8(+) T cells differentially mediate tumor control and respond to checkpoint blockade. Nat Immunol 20, 326–336 (2019). [PubMed: 30778252]
30. Chen Z, et al. TCF-1-Centered Transcriptional Network Drives an Effector versus Exhausted CD8 T Cell-Fate Decision. Immunity 51, 840–855 e845 (2019). [PubMed: 31606264]
31. Hudson WH, et al. Proliferating Transitory T Cells with an Effector-like Transcriptional Signature Emerge from PD-1(+) Stem-like CD8(+) T Cells during Chronic Infection. Immunity 51, 1043–1058 e1044 (2019). [PubMed: 31810882]
32. Zander R, et al. CD4(+) T Cell Help Is Required for the Formation of a Cytolytic CD8(+) T Cell Subset that Protects against Chronic Infection and Cancer. Immunity 51, 1028–1042 e1024 (2019). [PubMed: 31810883]
33. Lin H, et al. Host expression of PD-L1 determines efficacy of PD-L1 pathway blockade-mediated tumor regression. J Clin Invest 128, 805–815 (2018). [PubMed: 29337305]
34. Wen H, Dou Y, Hogaboam CM & Kunkel SL Epigenetic regulation of dendritic cell-derived interleukin-12 facilitates immunosuppression after a severe innate immune response. Blood 111, 1797–1804 (2008). [PubMed: 18055863]
35. Mo F, et al. An engineered IL-2 partial agonist promotes CD8(+) T cell stemness. Nature 597, 544–548 (2021). [PubMed: 34526724]
36. Spolski R, Li P & Leonard WJ Biology and regulation of IL-2: from molecular mechanisms to human therapy. Nat Rev Immunol 18, 648–659 (2018). [PubMed: 30089912]
37. Krieg C, Letourneau S, Pantaleo G & Boyman O Improved IL-2 immunotherapy by selective stimulation of IL-2 receptors on lymphocytes and endothelial cells. Proc Natl Acad Sci U S A 107, 11906–11911 (2010). [PubMed: 20547866]
38. Spangler JB, et al. Antibodies to Interleukin-2 Elicit Selective T Cell Subset Potentiation through Distinct Conformational Mechanisms. Immunity 42, 815–825 (2015). [PubMed: 25992858]
39. Chen J, et al. NR4A transcription factors limit CAR T cell function in solid tumours. Nature 567, 530–534 (2019). [PubMed: 30814732]
40. Ye L, et al. A genome-scale gain-of-function CRISPR screen in CD8 T cells identifies proline metabolism as a means to enhance CAR-T therapy. Cell Metab 34, 595–614 e514 (2022). [PubMed: 35276062]

41. Lotze MT, et al. High-dose recombinant interleukin 2 in the treatment of patients with disseminated cancer. Responses, treatment-related morbidity, and histologic findings. JAMA 256, 3117–3124 (1986). [PubMed: 3491225]
42. Dudley ME, et al. Cancer regression and autoimmunity in patients after clonal repopulation with antitumor lymphocytes. Science 298, 850–854 (2002). [PubMed: 12242449]
43. Hashimoto M, et al. CD8 T Cell Exhaustion in Chronic Infection and Cancer: Opportunities for Interventions. Annu Rev Med 69, 301–318 (2018). [PubMed: 29414259]
44. Beltra JC, et al. Developmental Relationships of Four Exhausted CD8(+) T Cell Subsets Reveals Underlying Transcriptional and Epigenetic Landscape Control Mechanisms. Immunity 52, 825–841 e828 (2020). [PubMed: 32396847]
45. West EE, et al. PD-L1 blockade synergizes with IL-2 therapy in reinvigorating exhausted T cells. J Clin Invest 123, 2604–2615 (2013). [PubMed: 23676462]
46. Wen H, Lei Y, Eun SY & Ting JP Plexin-A4-semaphorin 3A signaling is required for Toll-like receptor- and sepsis-induced cytokine storm. J Exp Med 207, 2943–2957 (2010). [PubMed: 21098092]
47. Kwon H, et al. Androgen conspires with the CD8(+) T cell exhaustion program and contributes to sex bias in cancer. Sci Immunol (2022).
48. Van Gassen S, et al. FlowSOM: Using self-organizing maps for visualization and interpretation of cytometry data. Cytometry A 87, 636–645 (2015). [PubMed: 25573116]
49. Zilionis R, et al. Single-cell barcoding and sequencing using droplet microfluidics. Nat Protoc 12, 44–73 (2017). [PubMed: 27929523]
50. Zuo D, et al. PlasmID: a centralized repository for plasmid clone information and distribution. Nucleic Acids Res 35, D680–684 (2007). [PubMed: 17132831]
51. Lin YH, et al. Self-Assembled STrap for Global Proteomics and Salivary Biomarker Discovery. J Proteome Res 18, 1907–1915 (2019). [PubMed: 30848925]
52. Tyanova S, Temu T & Cox J The MaxQuant computational platform for mass spectrometry-based shotgun proteomics. Nat Protoc 11, 2301–2319 (2016). [PubMed: 27809316]
53. Kochenderfer JN, Yu Z, Frasheri D, Restifo NP & Rosenberg SA Adoptive transfer of syngeneic T cells transduced with a chimeric antigen receptor that recognizes murine CD19 can eradicate lymphoma and normal B cells. Blood 116, 3875–3886 (2010). [PubMed: 20631379]

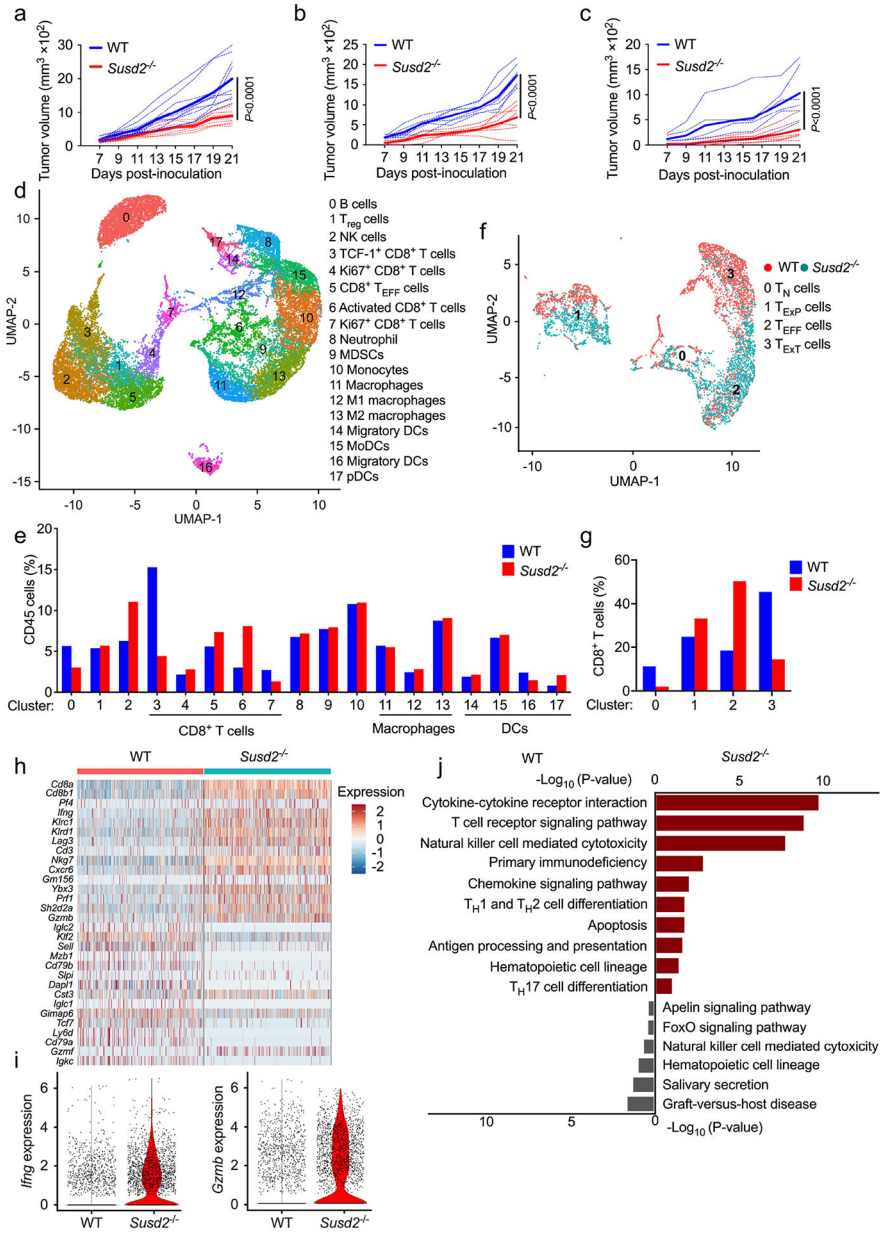

Figure 1. Genetic deletion of *Susd2* results in improved antitumor immunity.

a-c, Tumor growth at day 7, 9, 11, 13,15, 17, 19 and 21 post inoculation with MC38 **(a),** EG7 **(b)** or B16-OVA **(c)** tumor cells in wild-type (WT) and *Susd2*$^{-/-}$ mice. Dotted lines, values from individual mouse; solid lines, mean values. **d,e,** Uniform manifold approximation and projection (UMAP) of intratumoral CD45^{+} cells **(d)** and quantitation of each cell type **(e)** in WT and *Susd2*$^{-/-}$ mice at day 18 post-inoculation with MC38 tumors. **d,** Clusters denoted by color are labeled with inferred cell types. **f,g,** UMAP **(f)** and quantitation **(g)** of intratumoral *Cd8a*$^{+}$ *Trbc1*$^{+}$ *Trbc2*$^{+}$ cells in WT and *Susd2*$^{-/-}$ mice at day 18 post-inoculation with MC38 tumors. **f,** Clusters are labeled with inferred intratumoral CD8^{+} cell subtypes. **h,i,** Heatmap of differentially expressed genes between WT and *Susd2*$^{-/-}$ intratumoral CD8^{+} cells **(h)** and violin plots showing *Ifng* and *Gzmb*

expression in WT and *Susd2*$^{-/-}$ intratumoral CD8^{+} cells **(i)** from mice as in **d,e. j,** Gene Ontology (GO) enrichment in WT and *Susd2*$^{-/-}$ intratumoral CD8^{+} cells from mice as in **d,e.** Hypergeometric test was used for functional enrichment in Enrichr. All *P*-values were Benjamini-Hochberg adjusted for multiple comparisons. **a**, $n = 10$; **b,** $n = 7$; **c,** WT, $n = 6$, *Susd2*$^{-/-}$, $n = 7$. Data in **a-c** are representative of four independent experiments. Statistical significance was calculated with two-way ANOVA followed by Tukey's multiple comparisons test with *P* values noted in the figure **(a-c). d-j,** are representative of two independent experiments.

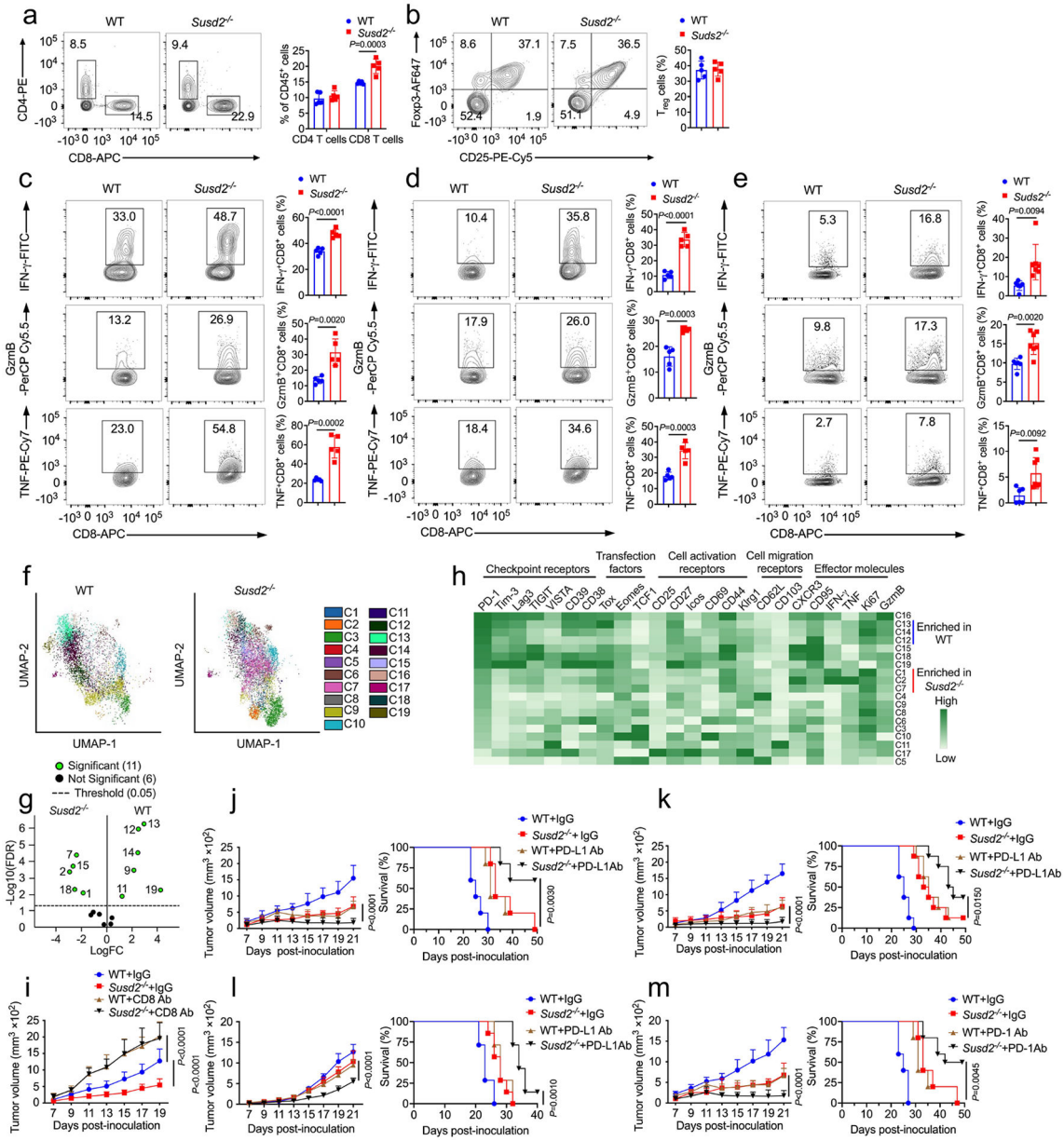

Figure 2. Enhanced antitumor response in *Susd2*$^{-/-}$ mice depends on CD8^{+} cells.

a,b, Flow cytometry analysis showing percentage of CD4^{+} and CD8^{+} T cells **(a)** and CD25^{+}Foxp3^{+} T_{reg} cells **(b)** in MC38 subcutaneous tumor isolated from WT or *Susd2*$^{-/-}$ mice at day 18 post-tumor inoculation **(a,b). c-e,** Flow cytometry analysis showing intracellular accumulation of IFN-γ, GzmB and TNF-expressing intratumoral CD8^{+} T cells in MC38 **(c),** EG7 **(d),** or B16-OVA **(e)** tumors isolated from WT or *Susd2*$^{-/-}$ mice at day 18 post-tumor inoculation. **f-h,** UMAP analysis **(f),** Volcano plot illustrating differential abundance clusters **(g)** and cluster-by-marker heatmap characterizing the expression patterns of individual clusters **(h)** of intratumoral CD8^{+} T cells from WT and *Susd2*$^{-/-}$ mice at day 18 post inoculation with MC38. **i,** Tumor growth in MC38-tumor bearing WT or *Susd2*$^{-/-}$ mice injected with either control IgG or CD8 Ab at day 0, 7 and 14 post tumor

inoculation. **j-l,** Tumor growth and survival in WT and *Susd2*$^{-/-}$ mice bearing either MC38 **(j),** EG7 **(k)** or B16-F10 **(l)** tumor cells injected with either control IgG or PD-L1 Ab at day 7, 10 and 13 after tumor inoculation. **m,** Tumor growth and survival in WT and *Susd2*$^{-/-}$ mice inoculated with MC38 tumor cells and injected with control IgG or PD-1 antibody at day7, 10 and 13 post tumor inoculation. **a-d,i,** $n = 5$; **e,** WT, $n = 6$, *Susd2*$^{-/-}$, $n = 7$; **f-h,k,** $n = 8$; l, $n = 7$; **j,m,** $n = 10$. n, number of mice per group. **a-e, i-m,** data are representative of three independent experiments; **f-h,** data are representative of two independent experiments. Statistical significance was determined by two-tailed unpaired Student's *t*-test **(a-e),** The *P* value was calculated using two-sided Wilcoxon's rank-sum test and adjusted with Bonferroni's correction **(g),** two-way ANOVA followed by Tukey's multiple comparisons test **(i,j left,l left,m left),** or Log-rank (Mantel-Cox) test survival analysis **(j right,l right,m right,)** with *P* values noted in the figure. The data represent mean ± SD.

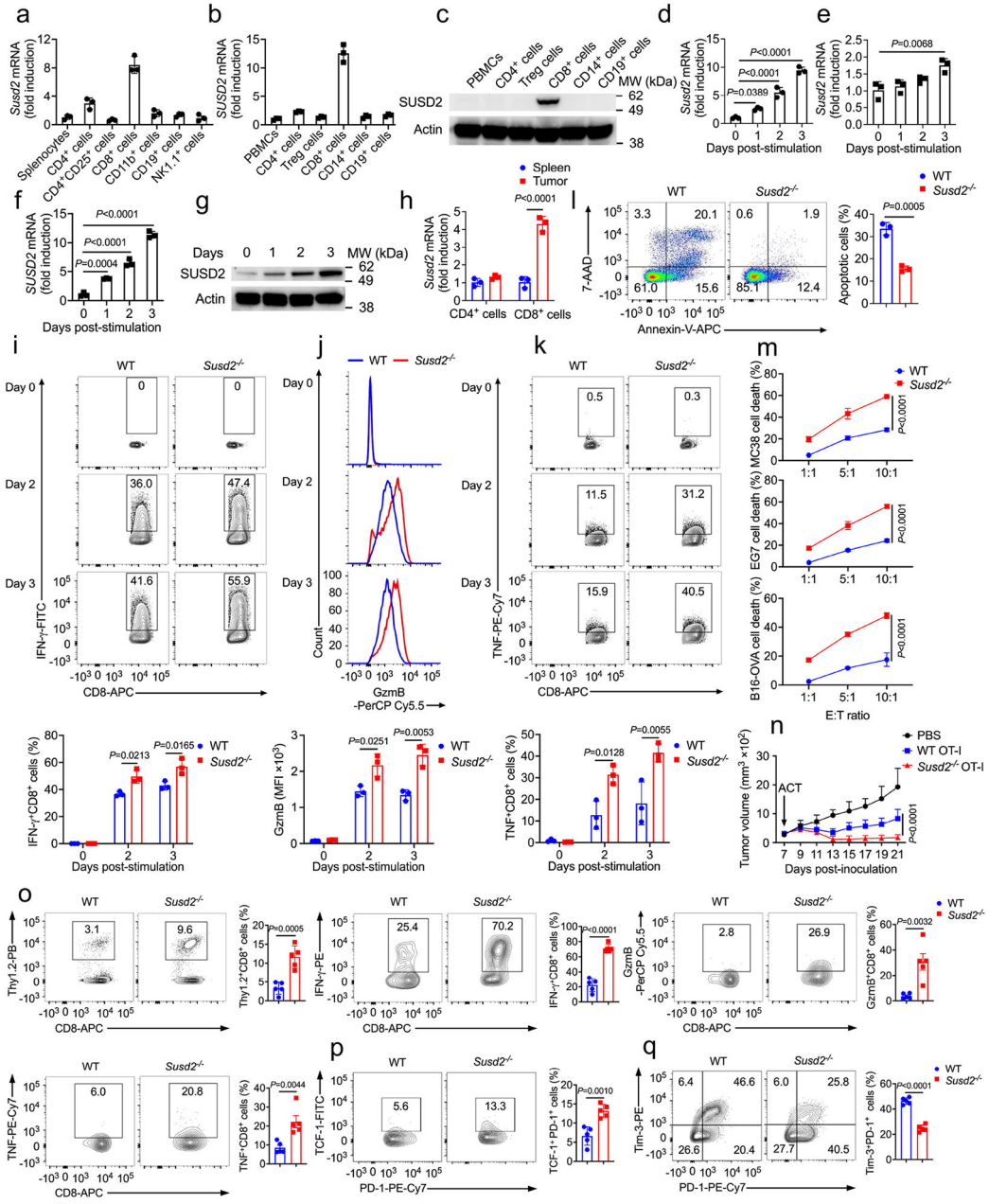

Figure 3. *Susd2*$^{-/-}$ CD8^{+} cells exhibit increased antitumor effector function and survival.

a-c, Transcript **(a,b)** and protein **(c)** of *SUSD2* in various immune cell types isolated from mouse spleen **(a)** or human PBMCs **(b,c). d-g,** Transcript **(d-f)** and protein **(g)** of *SUSD2* in sorted mouse CD8^{+} T cells, mouse CD4^{+} T cells and human CD8^{+} T cells that have been left untreated or stimulated with CD3-CD28 Abs. **h,** Expression of *Susd2* transcript in CD4^{+} and CD8^{+} T cells isolated from either spleen or tumor tissue in mice bearing MC38 tumor. **i-k,** Representative flow cytometry analysis showing IFN-γ^{+}CD8^{+} T cells, GzmB^{+}CD8^{+} T cells and TNF^{+}CD8^{+} T cells in OVA$_{257-264}$ stimulated splenocytes isolated from WT or *Susd2*$^{-/-}$ OT-I mice at day 0, 2 and 3. **l**, Flow cytometry analysis showing annexin V^{+}7-AAD^{+}CD8^{+} T cells in OVA$_{257-264}$ stimulated splenocytes isolated from WT or *Susd2*$^{-/-}$

OT-I mice at day 3. **m,** *In vitro* killing of $OVA_{257-264}$ peptide-pulsed MC38 (upper), EG7 (middle) and B16-OVA (lower) cells by WT or *Susd2*$^{-/-}$ OT-I T cells after co-culture for 4 h. **n,** Tumor growth in EG7 bearing mice post transferred with PBS, $OVA_{257-264}$ primed WT or *Susd2*$^{-/-}$ OT-I T cells. **o-q,** Flow cytometry analysis showing Thy1.2^{+}CD8^{+} T cells, IFN-γ^{+}CD8^{+} T cells, GzmB^{+}CD8^{+} T cells, TNF^{+}CD8^{+} T cells, TCF-1^{+}PD-1^{+}CD8^{+} T cells and Tim-3^{+}PD-1^{+}CD8^{+} T cells in EG7 isolated from $OVA_{257-264}$ primed WT or *Susd2*$^{-/-}$ OT-I T cells transferred tumor bearing mice at day 18 post tumor inoculation. TCF-1^{+}PD-1^{+}CD8^{+} T cells were gated from PD-1^{+}CD8^{+} T cells. **a,b,d-f,h-m,** $n = 3$; **n-q,** $n = 5$. *n*, number of mice per group. **a-h,n-q,** data are representative of three independent experiments; **i-m,** data are representative of four independent experiments. Statistical significance was determined by one-way ANOVA followed by Tukey's test **(a,b,d-f),** two-tailed unpaired Student's *t*-test **(l,o-q),** or two-way ANOVA followed by Sidak's multiple comparisons test **(h-k,m)** or Tukey's multiple comparisons test **(n)** with *P* values noted in the figure. The data represent mean ± SD.

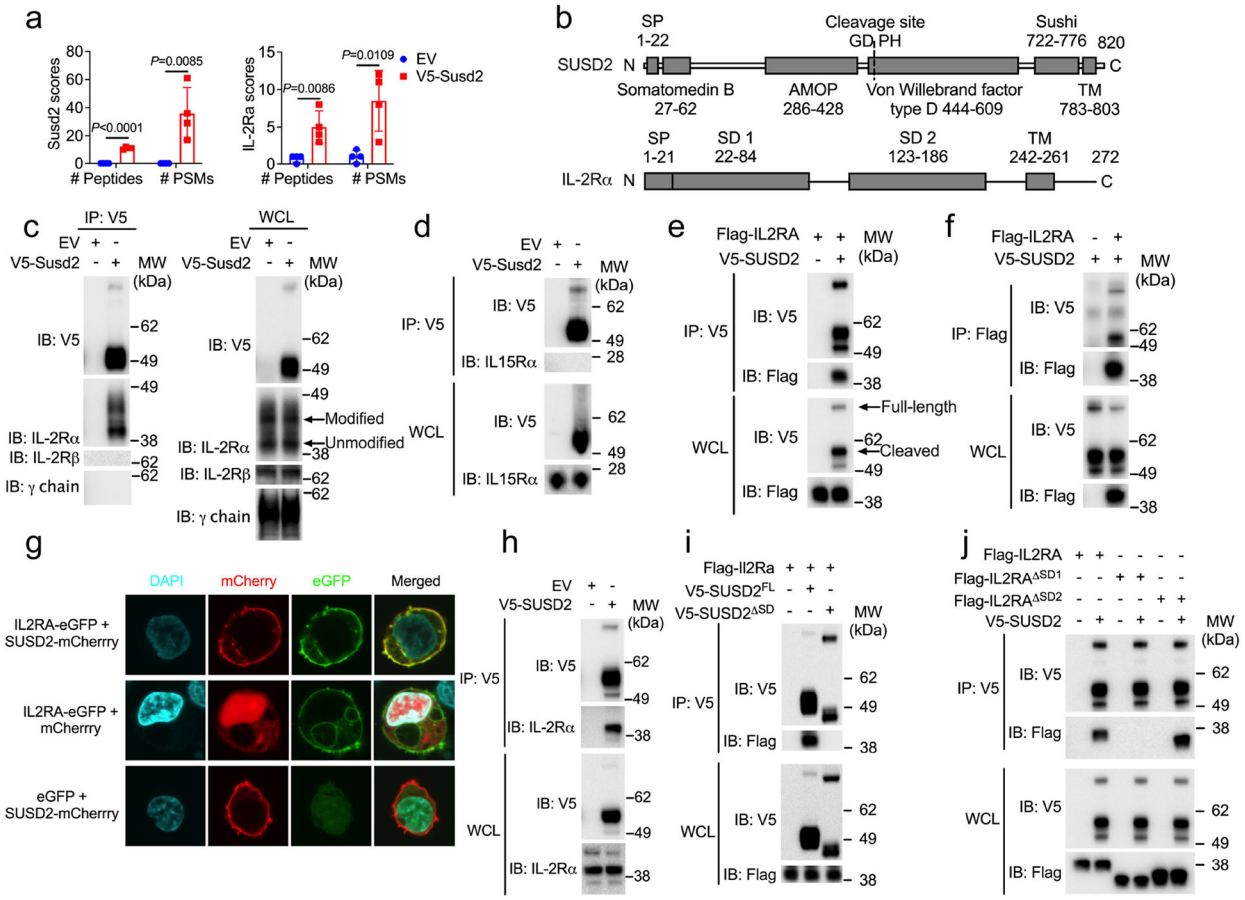

Figure 4. SUSD2 interacts with IL-2Rα via its sushi domain.

a, LC-MS/MS of Susd2-interacting proteins in Susd2-containing protein complex immunoprecipitated from *Susd2*$^{-/-}$ OT-I T cells reconstituted with either V5-tagged mouse *Susd2* or empty vector (PSMs, peptide-spectrum matches). **b,** Schematic domain structure of SUSD2 and IL-2Rα, SP, signal peptide, SD, sushi domain, TM, transmembrane domain. **c,d** Immunoblotting of IL-2Rα, IL-2Rβ or common γ chain **(c)** and IL-15Rα **(d)** in Susd2 precipitates immunoprecipitated from *Susd2*$^{-/-}$ OT-I T cells reconstituted with either empty vector or V5-tagged mouse *Susd2*. **e,f,** Immunoblot analysis of V5-SUSD2 and Flag-IL-2Rα in V5-SUSD2 or Flag-IL-2Rα precipitates immunoprecipitated from 293T cells transfected with V5-*SUSD2* and Flag-*IL2RA*. **g,** Immunofluorescence of 293T cells transfected with mCherry-SUSD2 and eGFP-IL2RA at 48 hours after transfection. **h,** Immunoblot analysis of SUSD2 and IL-2Rα in V5-SUSD2 precipitates immunoprecipitated from Jurkat T cells transduced with either V5-*SUSD2* or empty vector. **i,** Immunoblot analysis of V5-SUSD2^{FL}, V5-SUSD2$^{\Delta SD}$ and Flag-Il-2Rα in V5-SUSD2^{FL} or V5-SUSD2$^{\Delta SD}$ precipitates immunoprecipitated from 293T cells transfected with V5-*SUSD2*^{FL}, V5-*SUSD2*$^{\Delta SD}$ and Flag-*Il2rα*. **j,** Immunoblot analysis of V5-SUSD2, Flag-IL-2Rα, Flag-IL-2Rα^{SD1} and Flag-IL-2Rα^{SD2} in V5-SUSD2 precipitates immunoprecipitated from 293T cells transfected with V5-*SUSD2*, Flag-*Il2RA*, Flag-*Il2RA*$^{\Delta SD1}$ and Flag-*Il2RA*$^{\Delta SD2}$. **a,** $n = 4$. Bars show medians and symbols show individual mice. Statistical significance was determined by two-tailed unpaired Student's *t*-test with *P* values noted in the figure. Data in **a** are from two

independent experiments; **c-j,** data representative of three independent experiments. The data represent mean ± SD. WCL, Whole cell lysate, EV, Empty Vector.

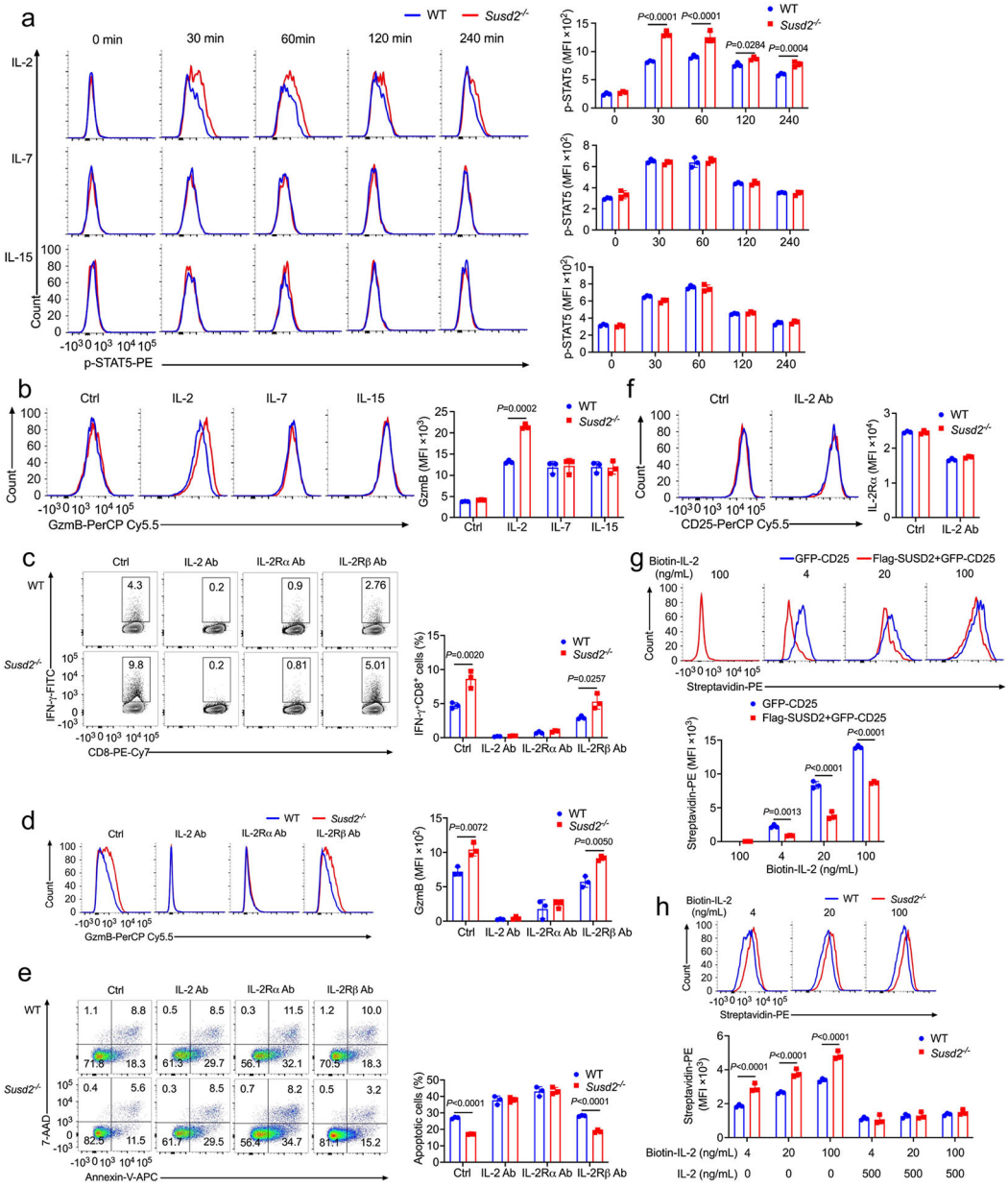

Figure 5. SUSD2 impairs CD8$^+$ cell effector function by attenuating IL-2Rα signaling.

a,b, Flow cytometry analysis of phosphorylated STAT5 (p-STAT5) **(a)** and intracellular GzmB **(b)** in $OVA_{257-264}$-primed WT or *Susd2*$^{-/-}$ OT-I T cells rested overnight and then stimulated with IL-2 (100 U/ml), IL-7 (5 ng/ml) or IL-15 (10 ng/ml) for 0, 30, 60, 120 and 240 minutes. **c-e,** Flow cytometry analysis of intracellular IFN-γ **(c),** GzmB **(d)** and cell apoptosis **(e)** in WT or *Susd2*$^{-/-}$ OT-I T cells stimulated with 200 ng/ml $OVA_{257-264}$ (suboptimal dose) for 48 hours. **f,** Flow cytometry analysis of IL-2Rα expression in $OVA_{257-264}$-stimulated WT or *Susd2*$^{-/-}$ OT-I T cells. **g,** Flow cytometry analysis of binding of biotinylated IL-2 on 293T cells overexpressing *SUSD2* and/or *IL2RA*. **h,** Flow cytometry analysis of biotinylated IL-2 binding to WT or *Susd2*$^{-/-}$ OT-I T cells treated or not with unconjugated IL-2. **a-h,** $n = 3$. *n*, number of mice per group. **a,b,g,h,** data

are representative of three independent experiments; **c-f,** data are representative of four independent experiments. Statistical significance was determined by two-way ANOVA followed by Sidak's multiple comparisons test **(a-h)** with *P* values noted in the figure. The data represent mean ± SD.

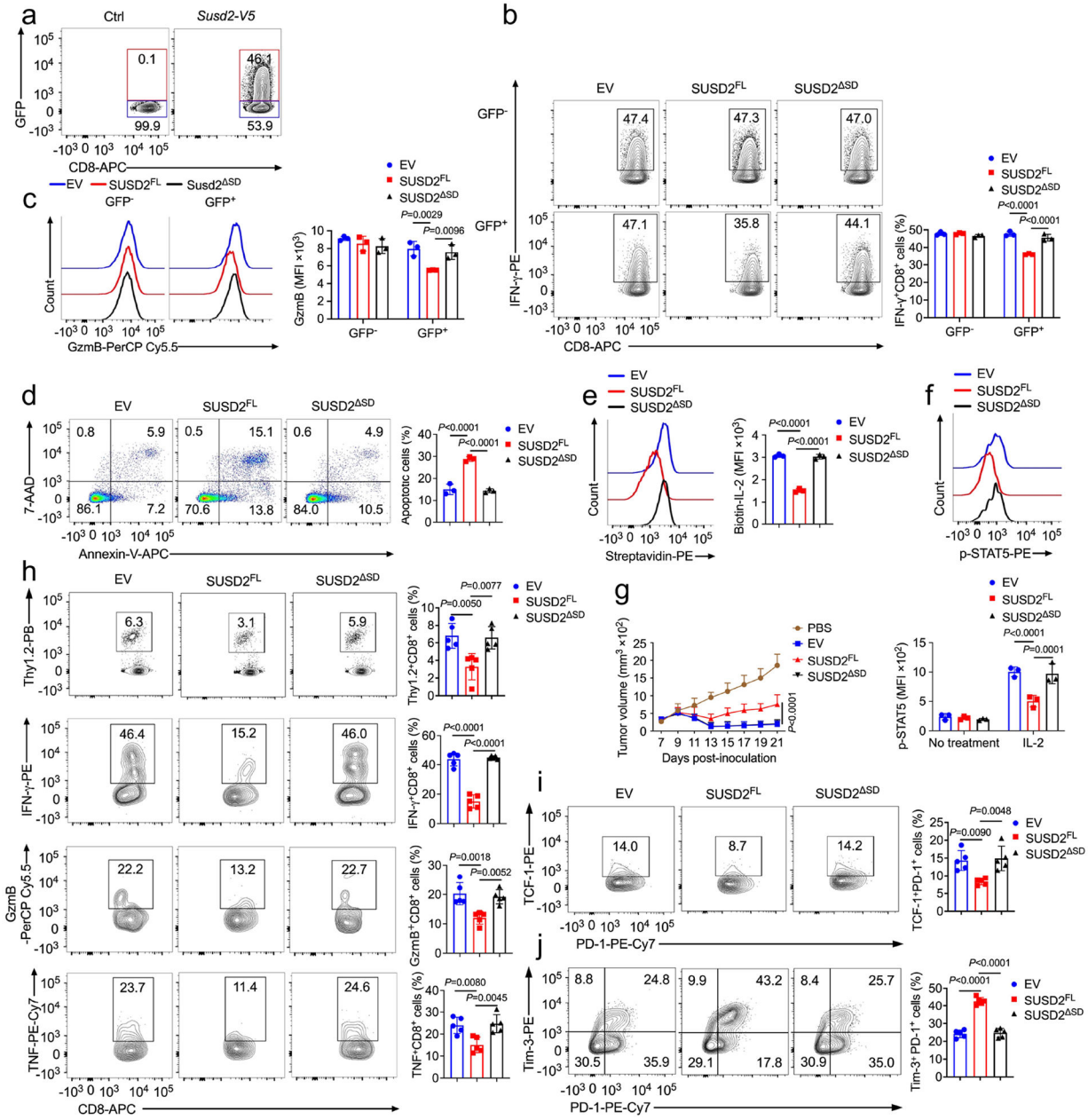

Figure 6. SUSD2-IL-2Rα interaction impairs antitumor effector function of CD8$^+$ T cells.

a, Flow cytometry analysis of GFP in OVA$_{257-264}$-primed *Susd2*$^{-/-}$ OT-I T cells transfected with EV-GFP or SUSD2^{FL}-GFP. **b-d,** Flow cytometry of IFN-γ$^+$CD8$^+$ T cells **(b),** GzmB$^+$CD8$^+$ T cells **(c)** and annexin-V$^+$7-AAD$^+$CD8$^+$ T cells **(d)** in OVA$_{257-264}$-stimulated *Susd2*$^{-/-}$ OT-I T cells retrovirally transduced with EV-GFP, SUSD2^{FL}-GFP or SUSD2$^{\Delta SD}$-GFP. **e,f,** Binding of biotinylated IL-2 assessed by streptavidin staining **(e)** and STAT5 phosphorylation **(f)** in OVA$_{257-264}$-primed *Susd2*$^{-/-}$ OT-I T cells retrovirally transduced with EV-GFP, SUSD2^{FL}-GFP or SUSD2$^{\Delta SD}$-GFP and stimulated with biotin-conjugated IL-2 for 1 h following overnight resting post-transduction. **g,** Tumor growth in EG7-bearing Thy1.1 congenic mice at day 2, 4, 6, 8, 10, 12 and 14 post PBS treatment or post-transfer

with *Susd2*$^{-/-}$ OT-I T cells transduced with EV-GFP, SUSD2^{FL}-GFP or SUSD2$^{\Delta SD}$-GFP. **h-j,** Frequencies of Thy1.2^{+}CD8^{+} T cells, IFN-γ^{+}CD8^{+} T cells, GzmB^{+}CD8^{+} T cells, TNF^{+}CD8^{+} T cells **(h),** TCF-1^{+}PD-1^{+}CD8^{+} T cells **(i)** and Tim-3^{+}PD-1^{+}CD8^{+} T cells **(j)** in EG7 tumors isolated at day 18 post EG7 inoculation from Thy1.1 mice that received *Susd2*$^{-/-}$ OT-I T cells transduced with EV-GFP, SUSD2^{FL}-GFP or SUSD2$^{\Delta SD}$-GFP at day 7 post EG7 inoculation. **a-f,** $n = 3$; **g-j,** $n = 5$. *n*, number of mice per group. **a-f,** data are representative of five independent experiments; **g-j,** data are representative of three independent experiments. Statistical significance was determined by two-way ANOVA followed by Tukey's multiple comparisons test **(b,c,f,g)** or one-way ANOVA followed by Tukey's test **(d,e,h-j)** with *P* values noted in the figure. The data represent mean ± SD.

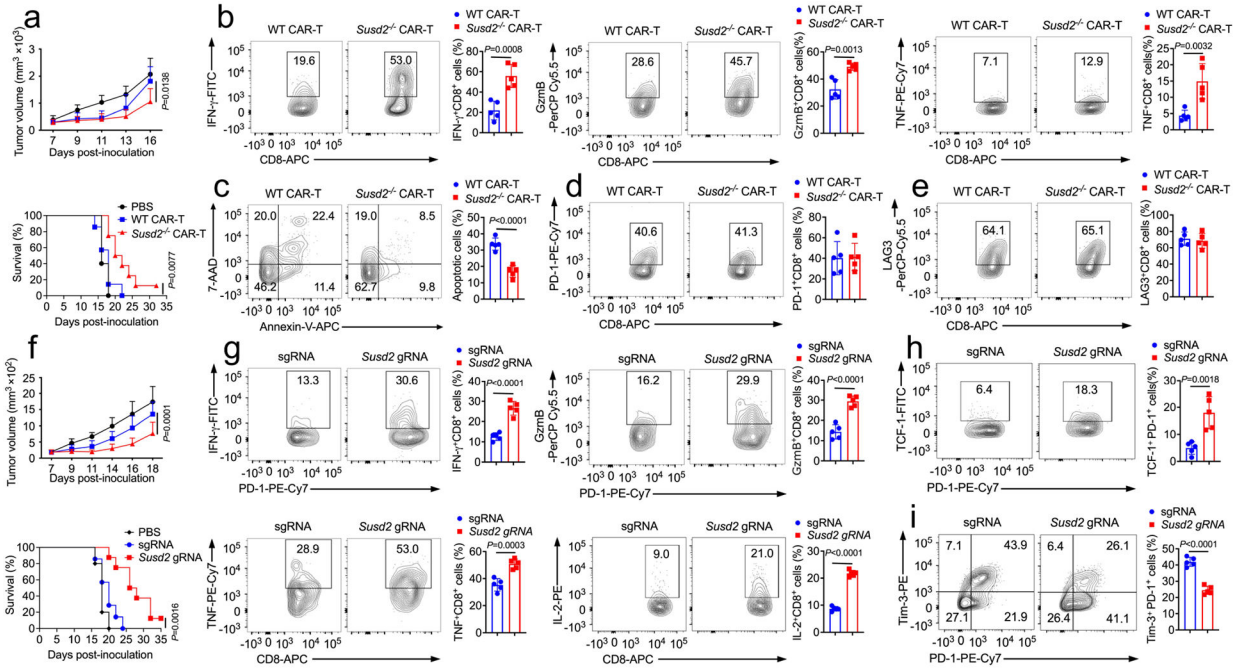

Figure 7. Deletion of Susd2 improves antitumor efficacy of CAR T cells.

a, Tumor growth and survival in EL4-hCD19 tumors-bearing *Rag2*$^{-/-}$ mice that received adoptive transfer of WT or *Susd2*$^{-/-}$ CAR T cells at day 7 post tumor inoculation. **b-e,** Frequencies of IFN-γ^{+}CD8^{+} T cells, GzmB^{+}CD8^{+} T cells, TNF^{+}CD8^{+} T cells **(b),** annexin V^{+}7-AAD^{+}CD8^{+} T cells **(c),** PD-1^{+}CD8^{+} T cells **(d)** and LAG3^{+}CD8^{+} T cells **(e)** in EL4-hCD19 tumors isolated from *Rag2*$^{-/-}$ mice that received WT or *Susd2*$^{-/-}$ CAR T cells at day 18 post tumor inoculation. **f,** Tumor growth and survival in EL4-hCD19-bearing *Rag2*$^{-/-}$ mice that received CAR T cells containing either scrambled gRNA (sgRNA) or *Susd2* gRNA at day 7 post tumor inoculation. **g-i,** Frequencies of IFN-γ^{+}CD8^{+} T cells, GzmB^{+}CD8^{+} T cells, TNF^{+}CD8^{+} T cells and IL-2^{+}CD8^{+} T cells **(g),** TCF-1^{+}PD-1^{+}CD8^{+} T cells **(h)** and Tim-3^{+}PD-1^{+}CD8^{+} T cells **(i)** in EL4-hCD19 tumors isolated from *Rag2*$^{-/-}$ mice transferred with sgRNA or *Susd2* gRNA CAR T cells at day 18 post tumor inoculation. **a**, n = 5-7; **f**, n = 5-8; **b-e**, **g-i**, n = 5. n, number of mice per group. **a-e**, data are representative of three independent experiments; **f-i**, data are representative of two independent experiments. Statistical significance was determined by two-way ANOVA followed by Tukey's multiple comparisons test (**a**,**f**, **top**), Log-rank (Mantel-Cox) test survival analysis (**a**,**f**, **bottom**) or two-tailed unpaired Student's *t*-test (**b-e**,**g-i**) with *P* values noted in the figure. The data represent mean ± SD.